Annals of Physics 490 (2026) 170473

Contents lists available at ScienceDirect

Annals of Physics

journal homepage: www.elsevier.com/locate/aop

Quantum phase diagrams and transitions for Chern topological insulators

Ralph M. Kaufmann [a,b,c,*], Mohamad Mousa [b], Birgit Wehefritz–Kaufmann [a,b,c]

[a] Department of Mathematics, Purdue University, West Lafayette, IN, 47907, USA
[b] Department of Physics and Astronomy, Purdue University, West Lafayette, IN, 47907, USA
[c] PQSEI, Purdue University, West Lafayette, IN, 47907, USA

ARTICLE INFO

Keywords:
Topological phases
Higher Chern numbers
Phase transitions
Lattices

ABSTRACT

Topological invariants such as Chern classes are central to the classification of topological phases. When system parameters vary, phase diagrams emerge in which these invariants can jump across critical loci, signaling a breakdown of topology. Our results place the behavior of Chern classes in phase diagrams on a robust theoretical foundation, unifying mathematical theory with concrete physical realizations. We give a fundamental mathematical analysis of this phenomenon and prove that any given abstract phase diagram of Chern phases can be realized through covering (winding) maps. The data of such a diagram can be given by specifying concrete physical systems with the given Chern classes. We provide examples of such systems, and construct explicit families exhibiting arbitrary Chern jumps, with critical loci governed by classical rose curves. These curves achieve the minimal number of Dirac points required, reflecting their role as local topological charges. Our analysis establishes this behavior as generic and unavoidable. To provide concrete condensed matter examples, we examine various lattices and tight-binding models, showing that effective winding maps—and hence higher Chern numbers—can be realized via kth nearest-neighbor couplings. We give explicit formulas for a family of 2D lattices using imaginary quadratic field extensions and their norms. Our study includes the square, triangular, honeycomb and Kagome lattices.

1. Introduction

Topological invariants have become a cornerstone of modern condensed matter physics [1–6]. Topological phases of matter are valuable due to the fact that global topological invariants produce robust, quantized behaviors—such as protected edge transport and non-Abelian quasiparticles, aka. anyons, that enable fault-tolerant quantum computing, ultra-low-dissipation electronics, and deeper theoretical insights into quantum field theory and condensed-matter physics. While topological phases are impervious to small perturbations, larger perturbation can lead to the breakdown of topological order, or in a phase transition to a new phase with a different topological order. Such phenomena are interesting as something to avoid in one type of scenario—for instance as they present a limit to fault tolerance. In other scenarios, understanding the parameters to be controlled to go through a phase transition is of paramount interest, such as in possible applications to quantum sensing. The best-known of these invariants are the Chern classes, especially the first, which has become central in the theory. When the appropriate bundle structure is identified, these cohomological classes can be assigned to physical systems, and integration produces the quantized invariants known as Chern numbers.

* Correspondence to: Purdue, Department of Mathematics, 150 N. University Street, West Lafayette, IN 47907, USA.
E-mail addresses: rkaufman@purdue.edu (R.M. Kaufmann), mmousa@purdue.edu (M. Mousa), ebkaufma@purdue.edu (B. Wehefritz–Kaufmann).

https://doi.org/10.1016/j.aop.2026.170473
Received 10 November 2025; Accepted 2 April 2026
Available online 11 April 2026

Going back to the fundamental insight of Berry [7], in non-degenerate systems, one can consider the line bundle defined by a non-degenerate state and the connection defined by adiabatic transport which exhibits a non-trivial holonomy. One can then integrate the associated Berry curvature to obtain a topological invariant, the Chern class. These invariants by another name are the TKNN numbers in the quantum Hall effect. These models have a quantized Hall conductivity given by the first Chern number [8]. Note that as Chern classes are topological invariants, they do not depend on the choice of the connection, and thus any convenient one can be used, see, e.g. Simon [9].

In condensed matter, natural line bundles of this type are provided by Bloch theory. The Brillouin zone serves as the base space for these bundles, while the fibers are given by the occupied bands, see e.g. [10]. Again, going back to Berry, interesting geometries, and with them interesting Chern invariants, appear in spin system realizations, see e.g. [11–13]. This is reviewed in §2.1. There is a dual C^*–perspective to this geometric setup which employs projectors to describe such Chern classes and K-theory of bundles [1,3]. The advantage of this approach is that it seamlessly extends to the noncommutative setting encountered in the presence of magnetic fields. It is also the natural setting for Harper Hamiltonians viewed as operators on a Hilbert space, as we review below in §4.1. These also allow for numerical treatment with such tools as the pseudospectrum [14].

After finding systems with non-trivial Chern numbers in condensed matter systems, such as the Haldane system [11] for Chern classes ± 1, a key area of active research is the realization of higher Chern numbers (i.e., with absolute value greater than one) and their appearance in phase diagrams of condensed matter systems. Studies in the physics literature suggested that introducing long-range interactions can give rise to higher Chern numbers. For example, [15] presents a systematic numerical and analytical extension of Haldane's graphene model, showing that the Chern number generally increases with the inclusion of more distant neighbor couplings. We are able to classify this behavior in several ways. The first is to realize that indeed passing to higher order neighbors increases the Chern number in a controlled way and the second is that even more control can be enforced by only looking at commensurate sublattices, that is those that are made up of n–the nearest neighbors and are homotheties of the original lattice, see §4.

Other approaches have also been proposed to realize higher Chern numbers in tight-binding lattices. One such strategy is to enlarge the unit cell by introducing additional orbitals, see [16], while another is to stack multiple layers of the system, see e.g. [17]. These two methods are closely related: stacking increases the number of atoms in the enlarged unit cell, and atoms from different layers can be interpreted as additional orbitals [18]. A range of studies has explored higher Chern numbers along these lines [15,18–29]. As we discuss, these physical realizations connect to the fundamental topology and geometry responsible for Chern classes. From this perspective, there are three standard operations for constructing bundles with higher Chern numbers: forming direct sums, taking tensor products, and performing pullbacks along higher-degree maps (see §2.1 for details). Physically, adding orbitals or stacking layers corresponds to taking direct sums, see also §2.2.1, and §4.1, while tensor products arise in certain coupled systems and projections such as in the 1-d system [30]. Pull-backs occur naturally when considering parameterized systems, slicing higher-dimensional systems, see §3.2, or employing super cells in the Brillouin zone, see §4.1.2 . Each of these operations has a well-defined effect on Chern numbers, providing a systematic way to generate and analyze higher Chern number phases.

An ensuing problem is what kind of topological phase transitions between phases with different Chern numbers are possible, and more generally, what type of phase diagram may appear. Leveraging the mathematical tools, we prove that *any* abstract quantum phase diagram in which the phases correspond to non-degenerate ground states with given Chern number can be realized using concrete standard families of Hamiltonians. The phase transition lines are required to be tame, that is be transformable into a polyhedral cone. This means that they are like chambers in a decomposition of space into cones, see Definition 3.1 for the technical details. In particular, one can use spin-systems and their pull-back. This provides a principled approach for designing such systems and has high potential for applications in condensed matter physics, quantum computation, and quantum sensing.

The relevant Hamiltonians are of the form $H : BZ \to Herm_d$ where the map originates from a Brillouin zone BZ, which in the results is any surface and $Herm_d$ are $d \times d$ matrices where d is the number of bands. The basic families are from $BZ = S^2$ or $T^2 = S^1 \times S^1$ and are of the form $f(\mathbf{k}) \cdot \boldsymbol{\sigma}$ where $f : BZ \to \mathbb{R}^3$ is a continuous function and $\boldsymbol{\sigma}$ is a spin–s representation of $su(2)$, most basically $spin = \frac{1}{2}$. Note there are two versions of the theory as we recall in §2.1, one purely topological, which is why the function only needs to be continuous. For the differential geometric formulation, one needs the notion of curvature, so the functions should be at least C^2, but often they are smooth, being polynomial or trigonometric. The latter appear naturally in tight-binding models. Mathematically, this corresponds to taking a character on the C^* algebra which typically sends a generator representing a translation operator along an edge to the function $e^{i\theta}$.

To explore concrete realizations in actual condensed matter systems, we then focus on the particular structure of 2D discrete tight-binding lattices that support topological insulating phases. In physical systems, interactions are generally local, and their strength depends on the Euclidean distance between lattice points. This motivates the systematic study of n–th neighbor commensurate sublattices, see §4.1.1. For these, the nth neighbor interaction is a just a rescaling $k_i \to Nk_i$ of the original action, where N is the distance of these neighbors. This yields a rescaling of the Chern number by $N^{\dim}$, where dim is the dimension of the system. In §5.1, we analyze several lattices representing concrete condensed matter systems, classify their commensurate sublattices, and show that these realizations are consistent with both the general mathematical constructions and the higher-order neighborhood models.

Roadmap to addressed problems and achieved results

We provide a complete framework combining all strands, partial answers and special constructions with new ideas and perspectives. In this way, our analysis is able to answer the following fundamental questions:

Q1: Which Chern classes and transitions are possible?
Q2: Which phase diagrams be realized, and can they be systematically designed?
Q3: Conversely, given a system, can the Chern classes and transitions be effectively understood and computed?
Q4: How can such phases be constructed in condensed matter by using lattices systems?

The answers we provide are as follows:

Answers to Q1:

(i) Arbitrarily high Chern numbers can appear as Chern roots realized by actual line bundles. These are already realized by basic spin Hamiltonians as studied by Berry [7], cf. §2.2.1.
(ii) Using Clebsch–Gordon rules, the bundles corresponding to higher spins can also be obtained from $spin\frac{1}{2}$, by using tensor products and projectors, see §2.2.1.
(iii) As a third option, we demonstrate that every Chern number and transition can be obtained by applying pull-backs along higher-degree covering maps to ± 1 Chern number $spin\frac{1}{2}$ systems, see Theorem 2.1. This universality is used in Theorem 2.2 to obtain a bundle with arbitrary Chern root line bundles.
(iv) We also give a concrete 1-parameter family of covering maps describing a single wall crossing from any given Chern number d to any given Chern number d'. This novel, exhaustive family of examples is realized by a suspension of a family of curves. The critical locus, i.e. the locus of the phase transition, is the suspension of the critical locus of the curve which is a classical rose curve $r = \cos(k\theta)$—whose history goes back to the 18th century [31]. We provide the link of the classical parameter k to the two Chern classes as $k = \frac{d-d'}{d+d'}$ and clarify that the curve in this setting is parameterized over $[0, |d - d'|\pi]$. A selection of interesting examples of such curves is collected in Fig. 1. The number of crossings, which are Dirac points in 2-band systems, is δ, which is the number of times $(0, 0)$ is crossed. This number is minimal for the two-band systems. Details are in §3.4.2.

Answers to Q2:

(i) As we demonstrate, any prescribed phase diagram of transitions between topological phases with different Chern numbers whose crossings are polytopic can be realized, see *Theorem* 3.1.
(ii) The key fact is that when the critical locus near a point of the phase diagram corresponds to a polytope fan, the standard wall-crossing families can be interpolated via the normal cone. For 2-band systems these standard families are minimal, in the sense that they realize the fewest possible level crossings (see §3.4.3).

Answers to Q3:

(i) Based on classical differential topology, the computation can be done via the curvature of a connection, using Chern–Weil theory. The adiabatic connection can be simulated.
(ii) In special cases, the bundle is a pull-back from a bundle with known Chern class, such as the bundles mentioned in the answer to Q1. The Chern number can then be computed via the mapping degree of the function which is used to pull-back.
(iii) The quickest computation of the degree is done with a ray method.

These results provided in §2.1.5 enable a direct interpretation and the "reading off" of the degrees and transitions, while simultaneously allowing for graphical representations; see §3.5.3 for examples.

Answers to Q4:

(i) The implementation is formally described by successive quotients by lattices and sublattices (see §4.1.2). Physically, this corresponds to including interaction terms with higher-order neighbors, which enables the realization of higher Chern numbers. The effects of moving to sublattices, or equivalently enlarging the unit cell, on the band structure—and hence on the topological properties—are discussed in §4.1.3.
(ii) Concretely, the theory is implemented in physical lattice systems by using commensurate lattices of higher order nearest neighbors, see §4.
(iii) A general blueprint for designing lattice systems with specific properties is given in §4.1.5.
(iv) We classify these for lattices formed by the integers $\mathcal{O}(\sqrt{-d})$ in imaginary quadratic field extensions in Appendix A. The results are summarized in Theorem 4.1. The method is to use knowledge about primes in these fields. These classifications let us identify infinite families of commensurate neighbors.
(v) For $d = 1$, these are the Gaussian integers, aka. the square lattice, and for $d = 3$ the Eisenstein integers, aka. the triangular lattice, see §5. We extend the analysis to sublattices, such as the hexagonal and Kagome lattices, see §5.1.

We also provide two appendices, Appendix A, which contains the background from number theory we use and Appendix B which contains numerical checks on the analytic theory we presented. We also give the pseudo-code for the ray method and address its stability.

2. Geometry

We introduce the geometric cast of characters for the analysis of topological phase diagrams.

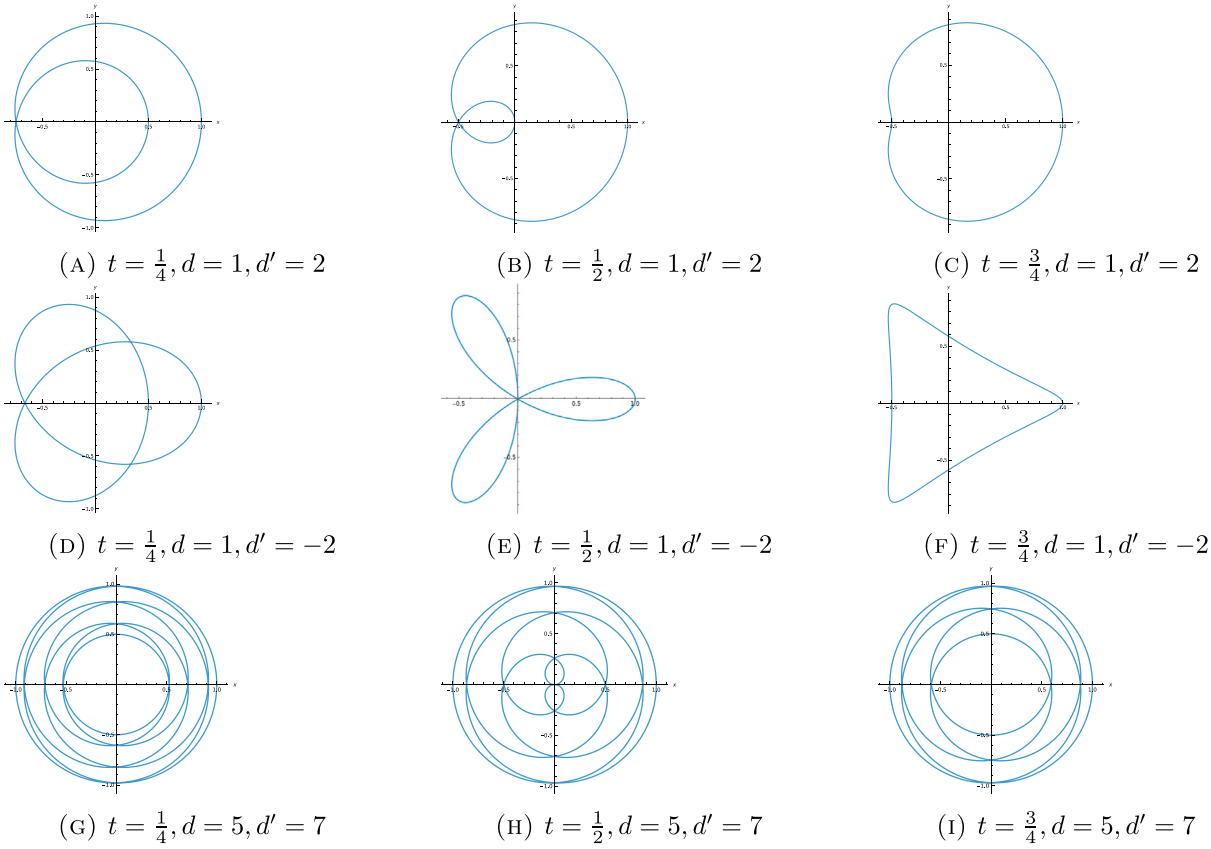

(A) $t = \frac{1}{4}, d = 1, d' = 2$ (B) $t = \frac{1}{2}, d = 1, d' = 2$ (C) $t = \frac{3}{4}, d = 1, d' = 2$

(D) $t = \frac{1}{4}, d = 1, d' = -2$ (E) $t = \frac{1}{2}, d = 1, d' = -2$ (F) $t = \frac{3}{4}, d = 1, d' = -2$

(G) $t = \frac{1}{4}, d = 5, d' = 7$ (H) $t = \frac{1}{2}, d = 5, d' = 7$ (I) $t = \frac{3}{4}, d = 5, d' = 7$

Fig. 1. Rose curves for different values of t, d and d'. The origin is in the image for $t = \frac{1}{2}$. The winding numbers are constant for $0 \leq t < \frac{1}{2}$ and $\frac{1}{2} < t \leq 1$. These can be readily be read off by using a ray.

2.1. Background

The following is a review of the material, we need to formally write and prove the statements. Although most of it is standard, we include the presentation for the sake of clarity and self-containment, assembling them here from various perspectives and sources.

2.1.1. Ground state line-bundle and n-band systems

Given a parameterized family of Hamiltonians, with a spectrum bounded from below, and a non-degenerate ground state, one obtains a line bundle of this ground state on the parameter space. This generalizes to the case of the lowest n bands, which form a rank n vector bundle. If the bands do not cross, the respective Eigenfunctions yield line bundles $L_i, i = 1, \dots, n$, and the vector bundle splits as $V = L_1 \oplus \cdots \oplus L_n$. In the standard condensed matter setup, V is the Bloch bundle and B is the Brillouin zone. The two standard cases for B are S^n, the n–sphere, and T^n, the n–torus.

2.1.2. Chern classes

The ith Chern class provides a cohomological invariant of a complex vector bundle $\pi : E \to B$, namely $c_i(E) \in H^{2i}(B, \mathbb{Z})$. It is convenient to put together the Chern classes into the *Chern polynomial*, $c_t(V) = \sum_k c_k(V) t^k$, where $c_0 = 1$. Note that there is a vanishing result for Chern classes which states that $c_i(E) = 0$ if $rk(E) < i$. Then the Chern classes satisfy $c_t(V \oplus W) = c_t(V) c_t(W)$. In particular, for a line bundle $c_t(L) = 1 + t c_1(L)$ and hence $c_1(L_1 \oplus L_2) = c_1(L_1) + c_1(L_2)$.

The *Chern character*, which is defined for a line bundle as $ch(L) = \exp(c_1(L))$ and then extended by the splitting principle, takes values in the even cohomology with $\mathbb{Q}$ (viz. rational) coefficients $H^{ev}(B, \mathbb{Q}) = \bigoplus_i H^{2i}(B, \mathbb{Q})$. That is, if $x_1, \dots x_n$ are the Chern roots of V —that is the formal roots $c_t(V) = \prod_j (1 + x_j t)$— then $ch(V) = \sum_j e^{x_i}$; the coefficients are elementary symmetric functions in the x_i which can be identified with Chern classes, see [32]. Expanding term by term $\mathrm{ch}(V) = \mathrm{rk}(V) + c_1(V) + \frac{1}{2}(c_1(V)^2 - 2c_2(V)) + \frac{1}{6}(c_1(V)^3 - 3c_1(V)c_2(V) + 3c_3(V)) + \cdots$. The Chern character is a ring homomorphism, i.e. it satisfies $ch(E \oplus F) = ch(E) + ch(F)$ and $ch(E \otimes F) = ch(E) ch(F)$ where the product is the cup product. From this it follows that for line bundles $c_1(L_1 \otimes L_2) = c_1(L_1) + c_1(L_2)$.

In the usual 2D case $B = S^2$ or T^2, the cohomology of degree bigger than 2 vanishes, and the only non-zero class is the class $c_1(E) \in H^2(S^2) \simeq \mathbb{Z}$ or respectively $c_1 \in H^2(T^2) \simeq \mathbb{Z}$. The isomorphism with $\mathbb{Z}$ is determined given by a choice of orientation.

By choosing this isomorphism, the invariant becomes integer-valued, the Chern number, which in physical terms is the topological charge. More generally, for a smooth oriented n dimensional connected manifold $H^n(M^n) \simeq \mathbb{Z}$. If M is even-dimensional $n = 2m$, the analogous Chern number is $c_m(V) \in H^{2m}(M^{2m}) \simeq \mathbb{Z}$. An orientation is given by a choice of the fundamental class $[M^n] \in H_n(B)$, and capping with the fundamental class $- \cap [M] : H^n(M) \to H^0(M) = \mathbb{Z}$ one obtains a Chern number. Moreover, since one can evaluate any degree n–cohomology class in this way, if $n = 2m$ is even and if $i_1 + i_2 + \cdots i_k = m$, then $(c_{i_1} \cup c_{i_2} \cdots \cup c_{i_k}) \cap [M] \in \mathbb{Z}$.

2.1.3. Chern–Weil theory

In physics the Chern numbers are obtained by integration. This is possible due to Chern–Weil theory which is available in the differentiable case, see e.g. [33]. Over $\mathbb{R}$, these cohomology classes have representatives in terms of differential forms of degree $2i$. Concretely, picking a connection ∇ and denoting its curvature form Ω, then $\det\left(\frac{i\Omega}{2\pi}t + I\right) = \sum_k c_k(V)t^k$. The surprising fact is that this is independent of the choice of connection. Using $det(X) = \exp(\mathrm{tr}(\ln(X)))$, the de Rham Chern forms which represent the Chern classes are explicitly given by

$$c_i^{dR}(V) = I + i\frac{\mathrm{tr}(\Omega)}{2\pi}t + \frac{\mathrm{tr}(\Omega^2) - \mathrm{tr}(\Omega)^2}{8\pi^2}t^2 + i\frac{-2\mathrm{tr}(\Omega^3) + 3\mathrm{tr}(\Omega^2)\mathrm{tr}(\Omega) - \mathrm{tr}(\Omega)^3}{48\pi^3}t^3 + \cdots \tag{1}$$

The Chern character in this notation is $ch(V) = \left[\mathrm{tr}\left(\exp\left(\frac{i\Omega}{2\pi}\right)\right)\right]$. If $\omega_1, \ldots \omega_m$ are the forms representing $c_i(E)$, then the cup product is given by the wedge product of forms and capping is given by integration. The Chern number is $\int_{[M]} \omega_{i_1} \wedge \ldots \omega_{i_k}$. The fact that these integrals are integers comes from the fact that the forms represent integer cohomology classes.

It is important to note that the Chern classes in cohomology and the Chern numbers *do not depend on the choice of connection*.

2.1.4. Pull-back and mapping degree

Being characteristic classes means that Chern classes behave well under pull-back. If $f : B' \to B$ is a continuous map, then $c_i(f^*(V)) = f^*(c_i(V))$, where on the left-hand side the bundle is pulled back and on the right-hand side the cohomology class is pulled back. This holds on the form level as well. Given a map $f : M^n \to N^n$ between two compact oriented n–manifolds, one can define the mapping degree by $f_*[M] = deg(f)[N]$, and for the Chern numbers we have $(f^*c_{i_1} \cup f^*c_{i_2} \cdots \cup f^*c_{i_k}) \cap [M] = deg(f)(c_{i_1} \cup c_{i_2} \cdots \cup c_{i_k}) \cap [N]$. Given a connected compact smooth n–dimensional Brillouin zone B^n, it can be realized as a CW complex with one top dimensional cell, and there is a canonical map of degree 1 to $\pi : B^n \to S^n$ given by collapsing the $n-1$ skeleton. For $B = T^2$ this is the collapse of the Fig. 8 given by $S^1 \vee S^1 = S^1 \times \{0\} \cup \{0\} \times S^1$.

In the non-compact case, one can compute the degree of a proper map using compactly supported forms [34]. This is needed if one thinks about maps to $\mathbb{R}^n \backslash \{O\}$. Any map from a compact manifold to $\mathbb{R}^n \backslash \{O\}$ is proper and one can compute the degree by pulling back a local generator which is given by a bump function. Hopf's Theorem [35] states that the mapping degree of a map $f : M \to S^n$ is a complete invariant for the homotopy groups $[M, S^n]$. In particular, the mapping degree of the map $f_d : z \to z^d : S^1 \to S^1 \subset \mathbb{C}$, or $\theta \mapsto d\theta$ in polar coordinates is of degree d and hence any map $f : S^1 \to S^1$ is homotopic to one of the maps f_d.

Concretely for the spaces T^2 and S^2, we can raise the Chern number by pulling back along the following maps: $f_{d_1,d_2} = f_{d_1} \times f_{d_2} : T^2 \to T^2, (\theta_1, \theta_2) \mapsto (d_1\theta_1, d_2\theta_2)$ whose degree is d_1d_2—this follows from the fact that the map f_d has degree d. A degree d map on S^2 is induced by the map f_d via suspension $Sf : SS^1 = S^2 \to SS^1 = S^2$. Recall that the suspension of a space is given by $SX = (X \times [0,1])/(X \times \{0\})\big/(X \times \{1\})$, viz. identifying $X \times \{0\}$ to one point and $X \times \{1\}$ to another. The suspension of a map is given by $f([x,t]) = [f(x), t]$. In particular, in spherical coordinates, Sz^d is the map $(\phi, \theta) \mapsto (d\phi, \theta) : SS^1 = S^2 \to SS^1 = S^2$. As the suspension of a homotopy yields a homotopy, it is a functor on spaces with homotopy equivalence classes of maps.

2.1.5. Calculating degrees

There are several ways to compute the mapping degree. For compact n–manifolds and $f : M^n \to N^n$, one can pull back any n–form ω, then $deg(f) = \frac{\int_M f^*\omega}{\int_N \omega}$. A standard choice for ω is the volume form. In particular, if $N = S^2$, $\omega = xdy\wedge dz - ydx\wedge dz + zdy\wedge dz$ is the standard volume form. Using spherical coordinates $\omega = \sin(\phi)d\phi \wedge d\theta$, one sees that the maps $S^2 \to S^2$ given by $(\phi, \theta) \mapsto (n\phi, m\theta)$ have degree nm. More generally, if f in a coordinate patch of N is given by $f(k_x, k_y) = (f_x, f_y, f_z) : T^2 \to S^2 \subset \mathbb{R}^3$, then $f^*\omega = f \cdot (\frac{\delta}{\delta k_x} f \times \frac{\delta}{\delta k_y} f)$. Given any map $h : N^2 \to \mathbb{R}^3 \setminus \{O\}$, we can normalize it to $f = \frac{h}{\|h\|}$ and then $deg(h) = deg(f)$. If for instance $M = T^2$ with coordinates k_x, k_y and $h : T^2 \to \mathbb{R}^3 \setminus \{O\}$, using $\int_{S^2} \omega = 4\pi$, we obtain:

$$deg(h) = deg(f) = \frac{1}{4\pi}\int_{\mathrm{T}^2} f \cdot \left(\partial_{k_x} f \times \partial_{k_y} f\right) dk_x\, dk_y \tag{2}$$

Another standard theory for computing the mapping degree is as follows, see e.g. [34, p 40ff], and [35]. By Sard's Theorem, the set of critical values of a smooth map $f : M \to N$ between two manifolds has measure zero. Picking a regular point q and a preimage p, the map f is a local diffeomorphism ϕ_p. Let $sgn(\phi_p) = \pm 1$ be the sign of the determinant of the Jacobian at p. I.e. 1 if ϕ_p preserves orientation and -1 if it reverses orientation. The mapping degree is then given by

$$\sum_{p \in f^{-1}(q)} sgn(\phi_p) \tag{3}$$

Note in the non-compact case f needs to be a proper map.

Using this method for a map $f : B^n \to \mathbb{R}^{n+1} \setminus \{O\}$ from an n–dimensional compact Brillouin zone B^n considered in the homotopy class $\tilde{f} \in [B^n, S^n]$, one has to identify the $p \in \tilde{f}^{-1}$ at a regular point and the local orientation at these points. By Sard's theorem the

regular points are generic. At these points, f is a local diffeomorphism and hence an immersion. At such points, one can use the ray method to compute the degree. For this consider the image $Im(f) \subset \mathbb{R}^3 \setminus \{O\}$ and a ray $R = (0,\infty)\mathbf{v}, \mathbf{v} \in S^2$ which intersects $Im(f)$ transversely outside the locus of self-intersections. Then there is a bijection of points $p \in \tilde{f}^{-1}(\mathbf{v}) \leftrightarrow R \cap Im(f)$. The local orientation can be found by computing the orientation of the frame $f_*(e_i), \mathbf{v}$ in $\mathbb{R}^{n+1}$, where e_i is a basis of TB_p. This also works for the self-intersection points, since for a local diffeomorphism, which is a local immersion, the ray has to intersect the image transversely only locally. For $B = S^n$ or $B = T^n$, the tangent bundle TB is stably trivial, so that by the Smale–Hirsch Theorem [36,37] one can homotope f to an immersion and compute the degree by using any ray.

In the physics literature the points $p \in \tilde{f}^{-1}(\mathbf{v}) \leftrightarrow R \cap Im(f)$, especially for the choice of the positive z-axis as the ray are sometimes called pre-Dirac points. For maps $B^n \to \mathbb{R}^{n+1}$, Dirac/Weyl points are the points in B^n that are preimages of the origin. Pre-Dirac points will already have two coordinates zero, whence the name. A technically more precise definition would be, points near the origin that in the limit of the phase transition have the origin as their limit.

Consider $g : B^n \to R^{n+1}\setminus\{O\} \sim S^n$—here and in the following $\sim$ means homotopic—and let $f = Sg$ for some $g : SB' \to \mathbb{R}^n\setminus\{O\} \sim S^{n-1}$, then by functoriality $deg(f) = deg(g)$, if one fixes that the fundamental class of B is the suspension of the fundamental class of B'. Specializing to a map $g : S^1 \to \mathbb{R}^2\setminus\{O\}$, we can see that $deg(g) = wind_0(g)$ is the classical winding number around 0 of g viewed as a closed curve which can be computed by the ray method with $\mathbf{v} \in S^1$. We then obtain $f \sim Sg : SS^1 = S^2 \to S(\mathbb{R}^2\setminus\{O\}) \sim SS^1 = S^2$, $deg(f) = deg(g)$.

In particular, if $\mathbb{R}^2 \cap im(f) = \bigcup_i c_i$, for at most transversely intersecting closed curves, and the c_i oriented so that the orientation of $(\mathbf{t}, \mathbf{v})$ is that of $(f_*(e_1), f_*(e_2), \mathbf{v})$, then $deg(f) = \sum_i wind_0(\pm c_i)$, which can be seen by using the ray method in $\mathbb{R}^3 \setminus \{O\}$ for a $\mathbf{v}$ in the equator of S^2. Note that if one does not fix the orientation, then the method only gives an integer mod 2, as one does not know the signs of the local contributions, cf. [35].

2.1.6. Momentum space and families of Hamiltonians

Consider a family of Hamiltonians depending on parameters in a base space B, that is $H : B \to Herm_d$. Note that any family is homotopic to a traceless family, and for non-degenerate families the homotopy can be chosen to stay in the space of non-degenerate families. The putative homotopy is given by $(1-t)H + t(H - \frac{1}{d}tr(H)I)$. The scaling has the effect of shifting all Eigenvalues by the same amount at the same time, so there are indeed no new crossings. Thus, we can assume that the families are traceless, when considering homotopy invariants.

Consider the trivial bundles $E = B \times \mathbb{C}^d \to B$. This has a fiberwise action $H(b) : E_b \to E_b : (b, v) \mapsto (b, H(b)v)$ and decomposes $E = \bigoplus_{i=1}^{l} V_i$ into block vector bundles V_i with $\sum_i rk(V_i) = d$, where the Eigenvalues in V_i and V_j never cross if $i \neq j$ and do cross inside the V_i. Let B_0 be the subspace on which the family is non-degenerate. For convenience and exposition, we will assume that B_0 has finitely many components. Over B_0 the bundle splits into line bundles $V = \bigoplus_{i=1}^{d} L_i$. As the total bundle is trivial, $\sum_i c_1(L_i) = 0$, see [10] for more details. On B_0, the topological invariants are then the Chern classes $c_1(L_i) \in H^2(B_0, \mathbb{Z})$. For a 2D connected compact component $B_0^i \subset B_0$, the Chern number of the nth band is $C_n^i = \frac{1}{2\pi}\int_{B_0^i} F_{12}(\mathbf{k})\, dS$, where $F_{12}(\mathbf{k}) = \frac{\partial}{\partial k_1}A_2(\mathbf{k}) - \frac{\partial}{\partial k_2}A_1(\mathbf{k})$ is the curvature (field strength tensor) of the connection A. With a Hermitian metric, one may choose the connection $A_\mu(\mathbf{k}) = -i\langle n_\mathbf{k} \mid \frac{\partial}{\partial k_\mu} n_\mathbf{k}\rangle$, where $|n_\mathbf{k}\rangle$ is a normalized local section (wavefunction) of the nth band. Such a choice is always possible, and the resulting Chern number is independent of this choice. For non-compact components, we proceed in the usual way by passing to their one-point compactifications.

Given a map $f : B' \to B$ and a family of Hamiltonians $B \to Herm_d$, we have the pull back family of Hamiltonians $f^*H = Hf : B' \to Herm_d$ given by $b \mapsto H(f(b))$. The bundles defined by this family are the pull backs under f of the bundles of the original family: i.e. if $V = \bigoplus_{i=1}^{d} L_i = B \times \mathbb{C}^d$, then $B' \times \mathbb{C}^d = \bigoplus_{i=1}^{d} f^*(L_i)$ with first Chern classes $f^*c_1(L_i)$ and Chern numbers $deg(f)c_1(L_i)$.

2.1.7. Families with degenerate locus

It is often assumed that $B_0 = B$, but since our aim is to study phase diagrams, we will also consider the case where degeneracies occur. As Chern numbers are topological invariants, observing phase transitions—detected as changes in Chern numbers when varying parameters—requires passing through families with a degenerate locus $B_{\text{deg}} = B \setminus B_0$. We will assume that B_{deg} is not too wild, in particular of at most codimension 1 —the technical details are in Definition 3.1. A previous systematic study is in [38]. If the bundle in question is given by a family of Hamiltonians, then

(1) Chern classes jump only when the degenerate locus is crossed. This happens when one closes a gap, and that is the description of a quantum phase transition. The jump of the Chern number is given by the local charge of the Dirac point defined in [38, Section 1.5]
(2) Generically the Chern numbers will jump by ± 1 for each gap closing at a non-higher-multiplicity point; see [38, Corollary 2.4].
(3) They can jump by multiples if either a non-transversal intersection point passes through the degenerate locus or several bands cross at once.

2.2. Standard examples with higher Chern numbers and universality

2.2.1. Spin Hamiltonians

The standard example of a Hamiltonian family is given by the family $H(\mathbf{k}) = \mathbf{k}\cdot\boldsymbol{\sigma}$, where $\boldsymbol{\sigma} = (\sigma_x, \sigma_y, \sigma_z)$ is a spin $s \in \mathbb{Z}[\frac{1}{2}]$ which is of dimension $d = 2s+1$. This is a family on $\mathbb{R}^3$ which is only degenerate at the origin. Restricting it to $S^2 \subset \mathbb{R}^3$, the trivial bundle $S^2 \times \mathbb{C}^d \to S^2$ splits as a direct sum of line bundles $L_i, i = -s, \dots, s$ corresponding to the Eigenvalues $-s, \dots, s$, whose Chern numbers are $\int_{S^2} c_1(L_i) = 2i$, [7,9]. The ground state bundle for this Hamiltonian has $c_1 = -2s$. Flipping H to $-H$, the ground state bundle has $c_1 = 2s$. Specializing to $s = \frac{1}{2}$, we obtain two bundles with Chern numbers ± 1. The bundle with Chern number 1 is classically known as the Hopf bundle. This is the associated vector bundle to the Hopf fibration $S^1 \to S^3 \to S^2$, aka. the Bloch sphere obtained by quotienting out a global phase from states in $\mathbb{C}^2$.

Thus there is a line bundle over S^2 with any given Chern number that comes from a Hamiltonian family. We can pull back this bundle to T^2 or any compact 2–dim connected BZ under the standard degree–1 map to S^2. This yields a line bundle over any such BZ with a specified Chern class.

One way to obtain higher spins is to take tensor products which are described by the Clebsch–Gordon rules. It suffices to start with $Spin\frac{1}{2}$ to obtain all possible isomorphism classes of line bundles. E.g. $Spin\frac{1}{2} \otimes Spin\frac{1}{2} = Spin\,1 \oplus Spin\,0$ where the first is a rank 3 bundle that splits into line bundles with Chern numbers $-2, 0, 2$ over S^2 and the second summand is a trivial line bundle. Namely, if L is the bundle with $c_1(L) = 1$ then $V = L \oplus \bar{L}$, $V \otimes V = (L \otimes L) \oplus (L \otimes \bar{L}) \oplus (\bar{L} \otimes L) \oplus (\bar{L} \otimes \bar{L})$ where the summands have first Chern numbers $1+1 = 2, 1-1 = 0, -1+1 = 0, -1-1 = -2$. Iterating this procedure produces arbitrarily high Chern numbers. In the Hamiltonian setting one simply takes the tensor product family $H(b) = H_1(b) \otimes H_2(b)$. Examples of such Hamiltonians are the 3+1 D Dirac Hamiltonian and the 8-component version, see e.g. [39, III.D.2]. (Note these are defined on subspaces of the full parameter space.)

2.2.2. Universality

More generally, we can pull back the standard spin–s representations as families $\mathbb{R}^3 \to Herm_d$, $d = 2s+1$ via maps $f : B \to \mathbb{R}^3$. For traceless 2×2, $d = 2, s = \frac{1}{2}$ families, the spin family is universal.

Theorem 2.1. *For any base space B, any given family of 2×2 Hermitian Hamiltonians $B \to Herm_2$ is homotopic to the standard family $H(\mathbf{k}) = \mathbf{k}\cdot\boldsymbol{\sigma}$, where $\boldsymbol{\sigma} = (\sigma_x, \sigma_y, \sigma_z)$ is given by the Pauli-matrices. And, moreover, non-degenerate families are pulled backs via maps $f : B \to \mathbb{R}^3 \setminus \{O\}$.*

Proof. The identity matrix $\sigma_0 = I$ and the Pauli matrices $\sigma_1, \sigma_2, \sigma_3$ are a basis of the Hermitian 2×2 matrices and the latter are a basis for the traceless Hermitian matrices. Using this basis, a map $H : B \to Herm_2$ can be written as $\sum_{i=0}^3 f_i\sigma_i$. The straight line homotopy $(1-t)f_0$ to 0 makes the map homotopic to $\sum_{i=1}^3 f_i\sigma_i$. The map $B \to \mathbb{R}^3$ is then given by $b \mapsto (f_1(b), f_2(b), f_3(b))$. The degenerate points in such a family are the inverse images of the origin O, as $\lambda_1 = \lambda_2 = -\lambda_1$ means that $\lambda_1 = \lambda_2 = 0$. □

Corollary 2.1. *The Chern numbers of the line bundles corresponding to non-degenerate 2×2 family of Hamiltonians on a base space B can be computed by pull back. In particular, if the base space is 2–dimensional, then c_1 can be computed as the mapping degree of the function f from the theorem above.*

For the mapping degree we note that $\mathbb{R}^3 \setminus \{O\}$ is homotopic to $[B, \mathbb{R}^3 \setminus \{O\}] \simeq [B, S^2]$. The map is induced by the homotopy $(1-t)f + tf/\|f\|$. The effect of this homotopy on H is spectral flattening, which means that the family of Hamiltonians is $(1-t)H + tH/|\lambda|$, where $\lambda, -\lambda$ are the Eigenvalues of H. The resulting Eigenvalues after the homotopy, that is at $t = 1$, are then just ± 1.

Corollary 2.2. *For any bundle V over a compact connected 2-manifold BZ that splits as a sum of line bundles $V \simeq L_1 \oplus \cdots \oplus L_n$ with first Chern classes $c_1^1, \dots, c_1^n$, there are functions $f_i : BZ \to S^2$ with $deg(f_i) = c_1^i$ such that $V \simeq \bigoplus_i f_i^*(H)$, where H is the Hopf bundle, that is the $-H_{spin\frac{1}{2}}$ ground state bundle. Alternatively, one can us the degree–1 map $\pi : BZ \to S^2$, $L_i = \pi^*(\tilde{L}_i)$ where $\tilde{L}_i = g^*_{c_1^i} H$. This can be identified with the highest state bundle of the spin $s = \frac{1}{2}c_1^i$ system.*

This in particular also allows to reconstruct bundles stemming from given families of Hamiltonians using pull-backs of pairs of line bundles stemming from $spin\frac{1}{2}$. As the total bundle is trivial in this case, the last line bundle L_d is equivalent to the quotient of the trivial d–dimensional bundle τ_d by $L_1 \oplus \cdots \oplus L_{d-1}$ which has first Chern number $-(c_1^1 + \cdots + c_1^{d-1})$.

Lemma 2.1. *Let $H \otimes \bar{H}$ be the bundles of the $spin\frac{1}{2}$ system, a fixed n and a collection of Chern numbers $c_1^i, i = 1, \dots n$ with $\sum_i c_1^i = 0$. Then*

$$H^{\otimes c_1^1} \oplus \cdots \oplus H^{\otimes c_1^{n-1}} \oplus (\bar{H}^{\otimes c_1^1} \otimes \cdots \otimes H^{\otimes c_1^{n-1}}) \tag{4}$$

is the trivial rank–n vector bundle over S^2 which splits as line bundles with the given Chern classes.

Proof. This follows from the fact that the bundle is $\bigoplus_{ij} H^{\otimes c_i^1} \otimes \bar{H}^{\otimes c_j^1}$ and $H \oplus \bar{H}$ is trivial. □

Theorem 2.2. *A given non-degenerate n–band structure $V = L_1 \oplus \cdots \oplus L_n \to BZ$, where L_1 are line bundles with Chern numbers c_1^i and V is trivial can be realized via $spin\frac{1}{2}$ bundles using the above construction.* □

This is commensurate with the analysis for $su(3)$ Hamiltonians yielding three-band models in [23].

3. Phase diagrams

We first present natural examples of phase diagrams, where the phases correspond to Chern phases of topological insulators, and then define the notion of an abstract phase diagram, which encompasses all such cases. We subsequently prove that any such abstract phase diagram can be realized by physical systems.

3.1. Phase diagrams from families of Hamiltonians

When dealing with families (or families of families) of Hamiltonians, one obtains phase diagrams. A natural setting is that one has a parameter space P which indexes Hamiltonians H_p in physical space. Each of these Hamiltonians gives a family $H_p(\mathbf{k})$ of d–dimensional Hermitian matrices with $\mathbf{k}$ in the physical Brillouin zone B. All in all, we obtain a family $P \times B \to Herm_d$. The dimensions of the parameter space P can be called synthetic dimensions in contrast to the real or momentum space dimensions represented by B. For instance in Example 3.2 the base space is T^2 spanned by the momenta (k_x, k_y) and the parameter space P is $\mathbb{R}^2$ spanned by the parameters (M, B).

At each point $p \in P$, we have the band structure of the family $H_p(\mathbf{k})$ as in §2.1, and if the ground state is non-degenerate, as it is for a Chern insulator, we have the first Chern class. In the case that B is a compact oriented surface, by integration over B this yields the first Chern number which, as it is a topological invariant, is a locally constant function of the parameters p. It will not be defined on the locus P_{deg}, where the ground state is degenerate, i.e. where we have a level crossing in the parameter space. In plots, these are the loci of the curves separating the regions with different Chern numbers.

3.2. Slicing and phase diagrams

Higher dimensional theories also naturally lead to phase diagrams. Given a family $B \to Herm_d$ without restriction on the dimension of B, as Chern classes lie in $H^{2i}(B, \mathbb{Z})$, to obtain a number, one in general has to pair with a degree $2i$ dimensional homology class. Such degree $2i$ classes arise from the embedding of $2i$–dimensional manifolds $j : N^{2i} \hookrightarrow B^m$. For these one can evaluate $c_i(j^*(L))$ as an integral: $\int_N j^*(c_i(V)) = \int_N c_i(j^*V)$. This works analogously for all Chern numbers. Thus, choosing a family of embeddings, parameterized by P, one obtains a phase diagram. The degenerate locus is comprised of those parameter values for which submanifold inclusions hit a degenerate point, i.e. $im(j) \cap B_{\text{deg}} \neq \emptyset$.

A typical situation which come from 3d lattices and is called slicing is given by an embedding $i_h : T^2 \hookrightarrow T^3 = T^2 \times S^1$ by $(\theta_1, \theta_2) \mapsto (\theta_1, \theta_2, h)$, with the parameter space being S^1. More generally, writing $T^n = T^{n-2} \times T^2$ with T^2 in the ith and kth slot $(i < k)$ we obtain $\binom{n}{2}$ families with $P = T^{n-2}$. This makes $n-2$ of the coordinates into parameters and reassigns them to be synthetic for the purposes of a phase diagram.

If the slices pass through the degenerate locus of the family, the Chern classes can jump, see [10,38] for detailed examples. If there are only finitely many degenerate points, then these numbers determine the class completely; see e.g. [10].

3.3. Abstract phase diagrams

Definition 3.1. An abstract n parameter quantum phase diagram PD will be given by a paracompact n–manifold P, together with a codimension–1 subspace P_{deg} such that $P_0 = P \setminus P_{deg}$ has finitely many components, and a locally constant function $C_1 : P_0 \to \mathbb{Z}$. We allow that multiple critical lines or codimension-1 degeneracy submanifolds meet, but the overall behavior is tame in the following technical sense. We restrict to the case where each point p of P_0 has a local neighborhood U that is homeomorphic to a neighborhood V of the origin in $\mathbb{R}^n$ with $U \cap B_0$ being homeomorphic to the codimension 1-cones of a polyhedral fan.

In 1D, locally P_{deg} is just the origin, while in 2D, locally P_{deg} can be the union of finitely many rays emanating from the origin. In 3D, locally, P_{deg} can be the union of finitely many boundaries of finitely many polyhedral cones of a complete fan, and so on. We recall that given a polyhedron which contains the origin, its fan has maximal cones given by the convex hull of the vertex vectors of each face of the polygon. The lower-dimensional cones are then the intersection of the higher-dimensional cones and correspond to the convex cones of the lower-dimensional faces.

We will deal with the 2D case for the Brillouin zone, i.e. BZ is a compact orientable surface. A family of Hamiltonians on a 2D Brillouin zone BZ parameterized by a manifold P *will be called tame*, if together with the locus P_{deg} and the locally-constant function $C_1 : P_0 \to \mathbb{Z}$ given by the first number of class of the line bundle of BZ defined by the ground state it yields the data of an abstract phase diagram.

3.4. Designing phase diagrams

Definition 3.2. Given an abstract phase diagram, a realization is a tame family of Hamiltonians and ground states parameterized by P which has the degenerate locus $P_{\deg}$ and regions with different phases classified by the Chern number function C_1. This means that for $p \in P_0$, $C_1(p)$ is the first Chern number of a non-degenerate ground state.

By designing a phase diagram, we mean specifying an abstract phase diagram and realizing it.

Theorem 3.1. *For any abstract phase diagram PD and any 2D compact oriented Brillouin zone BZ, there is a family of Hamiltonians parameterized by P whose phase diagram is PD, which, when on the wall between one domain with Chern number d and another domain with Chern number d' has $|d-d'|$ Dirac points. This gives an effective lower bound on the number of Dirac points, which is sharp for two-band systems.*

Proof. We first reduce to the case that $BZ = S^2$ by using the degree–1 map π obtained by collapsing the 1-skeleton of BZ.

The basic ingredient is the standard spin–$\frac{1}{2}$ family $H(\mathbf{k}) = -\mathbf{k}\cdot\boldsymbol{\sigma}$, which has Chern number $C_1 = 1$ for the ground state. We can change the Chern number to $C_1 = d$ by pulling back along a map $f_d : S^2 \to S^2$ of degree d. Note for concreteness, we can use $f_d = Sz^d$. These are the locally constant maps on the components of P_0. The local models at points $p \in B_{\deg}$ are given by the construction §3.4.1, and §3.4.3 below. We can glue these together using local partitions of unity.

These local models satisfy the condition for wall crossings, as the $\delta = |d-d'|$ points where the Hamiltonians are degenerate are indeed Dirac points. First, they are a discrete set, by [40, Theorem 1.2]. One can compute the local charges using the linear information [38, Corollary 2.4]. The sign of the linear information given by the sign of the Jacobian of the family around each level crossing, which is $\mathrm{sgn}(d'-d)$ and hence carries local charges ± 1. There are δ many of these points. These local charges correspond to the jumps in the Chern number along a path $[-\epsilon,\epsilon] \to P$ that passes through a wall, [10, §3.5.9.]. The minimum number of Dirac points needed is δ, which is attained. □

Note that the families from the Theorem are generic in the sense that on the wall, the level crossings are at isolated points, charges are ± 1, and there are no annihilations, that is, spurious Dirac pairs, or higher Chern number crossings. The latter two are non-generic, as can be seen from the characteristic map, see [40]. Without the extra conditions for wall crossings on the families, if P is metrizable, one can realize an abstract phase diagram by taking the families coming from pull-back with f_d inside the connected components and then scaling them by the distance to the degenerate locus. Each $\tilde{f_d}(p) = \inf_{q\in P_{\deg}} dist(p,q) f_d(p)$ will then go smoothly to zero on the walls; consequently will have a continuum of fully degenerate Hamiltonians, i.e. all Eigenvalues are 0, in these families if the walls are of positive dimension. Non-generic crossings do appear in real systems, for instance, in the Kagome lattice, see §5.1.9, which exhibits 2-band crossings with local charge 2, and the Gyroid, which has spin 1 points, that is 3–band crossings, see [38].

3.4.1. Wall crossings

Let $I = [0,1]$. The following construction gives rise to families on $I \times S^2$ regarded as a one-parameter family. To get a phase transition from Chern number d to d' consider $F = [(1-t)f_d + tf_{d'}] : I \times S^2 \to B^3$, where B^3 is the 3-ball, that interpolates between a degree d map $f_d : S^2 \to S^2 \subset \mathbb{R}^3 \setminus \{O\}$ and a degree d' map $f_{d'} : S^2 \to S^2 \subset \mathbb{R}^3 \setminus \{O\}$. If for some p, $[(1-t)f_d(p) + tf_{d'}(p)] = O$, then $(1-t)f_d(p) = -tf_{d'}(p)$, and since $\|f_d(p)\| = \|f_{d'}(p)\| = 1$ after taking norms this means that $1-t = t$ and hence $t = \frac{1}{2}$. Also, at $t = \frac{1}{2}$ there must be some p where $F(\frac{1}{2}, p) = 0$, because otherwise the degree cannot change.

Reparameterizing $[0,1]$ to $[-1,1]$ we can pull back this family to neighborhoods of points in $p \in P_{\deg}$ which locally are modeled by two regions in R^d separated by the wall $x_d = 0$, by pulling back along the projection $\pi_2 : R^{d-1} \times I \to I$.

3.4.2. Standard wall crossing and rose curves

For the 1-parameter crossing, choosing the standard maps $f_d = Sz^d$, where $z = e^{i\phi} \in S^1 \subset \mathbb{C}$, we have that $F = SG$ where $G(t,z) = [(1-t)z^d + tz^{d'}]$ as a map $[0,1] \times S^1 \to \mathbb{R}^2$. Now $G(t,z) = (0,0)$ if and only if $t = \frac{1}{2}$, and in this case, the curve is $G(\frac{1}{2}, z) = g(z) = \frac{1}{2}[z^d + z^{d'}]$. The number of times that the curve passes through zero, that is, the number of Dirac points, is given as $\delta = |d-d'|$. This is seen by noting that $z^d + z^{d'} = 0$ if and only if $z^\delta = -1$ whose solutions are the odd powers of a primitive 2δ–th roots of unity $\exp(i\frac{2\pi}{2\delta}(2k+1))$, $k = 0,\dots,\delta-1$. Physically, this means that the family has δ crossings corresponding to Dirac points. These happen at Eigenvalues $\lambda = 0$. Interpreting λ as the energy, and setting the Fermi level $E_F = 0$, as is common in systems such as graphene or Weyl semimetals, δ is the intersection with the Fermi energy, which can, in turn, be identified with the spectral flow [41]. Tracking the family in $\mathbb{R}^2$, one can also view the effect as pulling $|d-d'|$ strands through 0, or, alternatively, by tracking the change of the reference point pulling the origin through $|d-d'|$ strands to change the winding number by one unit for every strand, respectively point, following the behavior of the winding number. Thus $|d-d'|$ is an upper bound on the minimal number of Dirac points in a wall crossing. As the jumps from local charges in a 2-band system are only by ± 1 for each Dirac point, the number is minimal for these systems and the family provides the minimal model for the phase transition.

Rewriting in real coordinates, We get the equations

$$g(\phi) = (\cos(\frac{d-d'}{2}\phi)\cos(\frac{d+d'}{2}\phi), \cos(\frac{d-d'}{2})\sin(\frac{d+d'}{2}\phi)) \tag{5}$$

This is part of a classical curve called the rose curve, i.e. it satisfies the polar equation $r = \cos(k\theta)$ with $k = |\frac{d-d'}{d+d'}|$, if $d \neq -d'$. This is seen by computing $r^2 = g(z)\overline{g(z)}$ and $\theta = \arctan[\Im(g(z))/\Re(g(z))]$. The parameterized curve is parameterized either in the parameter $\phi \in [0, 2\pi]$ or in the parameter $\theta = \frac{d_1+d_2}{2} \in [0, (d_1 + d_2)\pi]$. To transverse a rose with $k = \frac{r}{s}$ With $gcd(r, s) = 1$ exactly once fully, one needs to work in the interval $[0, 2s]$ if both r and s are odd and $[0, s]$ else.

Examples: In the case $d = 0$, $k = 0$ the curve is simply the circle $\frac{1}{2} + \frac{1}{2}z$ of radius $\frac{1}{2}$ centered at $(\frac{1}{2}, 0)$. This is traversed d times—to go around once one needs the interval $[0, \pi]$, and the interval of θ is $[0, d\pi]$. If $d = -d'$, the curve collapses to the curve $(\cos(d\phi), 0)$ at the parameter $t = \frac{1}{2}$. Note that this passes through $(0, 0)$ exactly 2d times. In particular, for $d = 1$ this is at $(\frac{\pi}{2}, \frac{3\pi}{2})$. For the special case $d = 1, d' = 2$ we have $k = -\frac{1}{3}$ and the curve is the limaçon trisectrix on the interval $[0, 3\pi]$ which traverses the whole curve once, hitting the origin once. For $d = 1, d' = -2$, $k = -3$, and the curve is the trifolium, for the interval $[0, \pi]$, which traverses the curve once and passes three times through the origin. For $d = -2, d' = 4$, $k = \frac{-6}{2} = -3$ we again get the trifolium, but now on the interval $[0, 2\pi]$ which traverses the trifolium twice and passes six times through the origin. These examples are given in Fig. 1.

3.4.3. Polyhedral cones

If the local structure near $p \in P_{\deg}$ is given by the polytope P, then let N be the normal fan, [42, 7.1]. This is the fan in the dual space $(\mathbb{R}^d)^*$ consisting of the cones $\{C_F\}_{F \in \text{face}(P)}$ where $C_F = \{w \in (\mathbb{R}^d)^* \mid F\} \subseteq \{x \in P : w(x) = max_{y \in P} w(y)\}$. This is also the face fan of its polar polytope, [42, 7.3]. If the convex generators for C_F are $v_1, \dots, v_k$, we define the pull-back function as $\sum_{i=1}^k t_i f_i$, where f_i is the given function for the cone which is dual to the ray v_i and t_i are the coordinate functions of C_F, i.e. those defined by $p = \sum_{i=1}^k t_i(p) v_i$. This realizes all wall crossings at once.

3.5. Discussion, variants and examples

3.5.1. Discussion

This construction can be pulled back to T^2 using the collapse map $T^2 \to S^2$ and thus gives physical Hamiltonians depending on two generalized momenta.

If we already have a given Chern–number 1 family $H(\mathbf{k}) : T^2 \to Herm_d$, we can use $f_{d_1,d_2} : T^2 \to T^2, (\theta_1, \theta_2) \mapsto (d_1\theta_1, d_2\theta_2)$ whose degree is $d_1 d_2$ to provide Hamiltonians for the connected components of P_0 and then use the same argument as in the proof of Theorem 3.1 to obtain a family consisting solely of combinations of these pull-back Hamiltonians. The extra difficulty is to find the transition line of gap closings, if one does not simply scale to 0 when approaching the boundary as formalized in §3.5.2. If the original Hamiltonian is a two-band system of the form $H = f(k_x, k_y) \cdot \boldsymbol{\sigma}$, then the pulled back Hamiltonian has the form $H_{d_1,d_2} = f(d_1 k_x, d_2 k_y) \cdot \boldsymbol{\sigma}$. A wall crossing would be given by $H(t) = [(1-t) f(d_1 k_x, d_2 k_y) + t f(d_1' k_x, d_2' k_y)] \cdot \boldsymbol{\sigma}$. Now the critical locus where the Hamiltonian is degenerate is given by $[(1-t) f(d_1 k_x, d_2 k_y) + t f(d_1' k_x, d_2' k_y)] = 0$ which occurs at values $t = \frac{f(d_1 k_x, d_2 k_y)}{f(d_1 k_x, d_2 k_y) - f(d_1' k_x, d_2' k_y)}$ provided that the numerator is not zero, and if the numerator is zero at roots $f(d_1 k_x, d_2 k_y) = 0$. The particularities then depend on the function f, as do the particular local charges. The analysis of the local charges that appear for any finite number of bands is then encoded in the characteristic map of [40], which can be very complex.

In particular, in §4 below, we give lattice Hamiltonians realizing infinite sets of Chern numbers using pull–backs $f_{d,d}$. These are the pull-back corresponding to commensurate lattices, that is, using the same lattice geometry up to homothety, see §5.1. This means that these are local Harper Hamiltonians whose periodicity is the one of the sublattice. This is the situation described in §4.1.2, and the locality is scaled by d.

If the abstract diagram only contains Chern numbers from these sets, we can use combinations of these specific Hamiltonians, which are all local. The combinations are simply linear for wall crossings and, in the polytope version, can be chosen to be piecewise linear. In general, the partition of unity acts as a tuning parameter. The actual wall crossings are then not bound to be hyperplanes or polytopal, like in Theorem 3.1, cf. §3.4.3.

Thus, the minimality condition of using ± 1 charge Dirac points is an extra condition. In many given systems, the phase diagram can involve higher charge Dirac points. See §5.1.9 or [38]. Theorem 3.1 is an existence theorem. Note that the basic input system that is needed is the physical system $\mathbf{k} \cdot \boldsymbol{\sigma}$. One can ask to choose from a different set of physical systems, for instance lattice models. This is addressed in §4, which also contains specific models.

3.5.2. Different covering maps and non-minimal transitions

One can, of course, use any maps of the given degrees, not just the suspension maps, to define the straight line homotopy F. In the case of a jump from $+1$ to -1, we can use the identity id as the degree–1 map and any map with image S^2 which is degree -1 when restricted to its image. The two standard choices for this are the antipodal map $a : \mathbf{k} \to -\mathbf{k}$ or the map $a_z : (k_x, k_y, k_z) \to (k_x, k_y, -k_z)$. For a, there is a singularity at $t = 1/2$ where the whole map collapses to the origin $F(1/2, \mathbf{k}) \equiv O$. For $t \neq 1/2$ the image is in $\mathbb{R}^3 \setminus \{O\}$ and the map has a mapping degree, which is $1, t < 1/2$ and $-1, t > 1/2$. We obtain the family $(1-2t)\mathbf{k} = \alpha \mathbf{k}$, where $\alpha = 1 - 2t \in [-1, 1]$. As $\frac{|\alpha|}{2}$ is the distance of t to $\frac{1}{2}$ this is an example of scaling the map to zero at the critical locus.

In the second case, also for $t \neq 1/2$, the image is in $\mathbb{R}^3 \setminus \{O\}$ and the map has a mapping degree, which is $1, t < 1/2$ and $-1, t > 1/2$. For $t = 1/2$, the image is the standard disc which contains the origin O. Writing this as

$$k_x \sigma_x + k_y \sigma_y + m \sigma_z \tag{6}$$

where $m = (1 - 2t)k_z$, we see that the mass gap vanishes at $t = 1/2$. This particular model appears as a Dirac model, cf. [41, 2.3]. Note that in both cases, there is a band crossing at the critical point, O is in the image, and this has to be the case, since otherwise the Chern class would be invariant. The perceived contradiction is lifted by the fact that there is no splitting for the two line bundles involved in the crossing, if a crossing point is present, see [38] for further discussions.

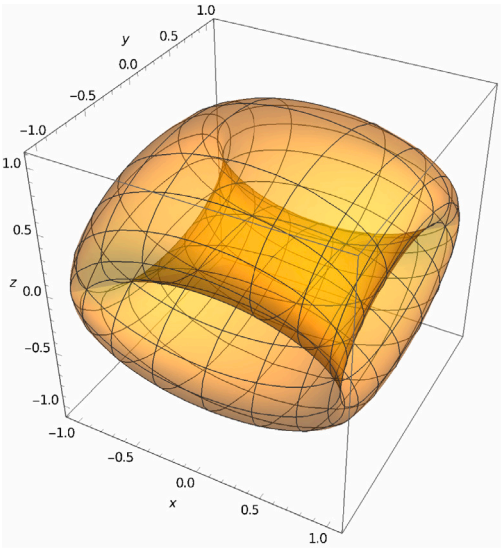

Fig. 2. Surface plot of the function given in Eq. (7) for $M = B = 1$. Increasing M moves the surface up, and decreasing M moves it down. This is the phase transition between regions 1 and 2 in Fig. 3, see also Table 1.

3.5.3. *Explicit continuum examples*

Example 3.1. We illustrate the construction §3.4.3 for a 2-parameter family with k rays. Up to isotopy, fixing the origin and the incidence relations, we can arrange the rays to be in the directions of the k–th roots of unity ζ_k. Then the normal cone is given by the odd $2k$–th roots ζ_{2k}^{2n+1}. If in the chamber between ζ_k^{i-1} and ζ_k^i the $C_1 = d_i$, then in the chamber between ζ_{2k}^{2i-1} and ζ_{2k}^{2i+1} for $p = a_1\zeta_{2k}^{2i-1} + a_2\zeta_{2k}^{2i+1}$ the function F is given by $a_1(p)f_{d_i} + a_2(p)f_{d_{i+1}}$. Similar to the 1-parameter calculation, $F(p) = O$ means that $a_1(p) = a_2(p)$ and hence p is on the ray $\zeta_{2k}^{2i} = \zeta_k^i$ and hence is on the critical locus.

Example 3.2. To demonstrate the efficacy of the ray method, and give a concrete example with parameter space $\mathbb{R}^2$, and base space T^2, we now consider a specific 2-parameter model coming from spin–orbit coupling, cf. [41], this goes back to a similar Hamiltonian in [43] used to describe the spin-Hall effect.

$$H(\mathbf{k}) = (\sin(k_x), \sin(k_y)), M - B(\sin^2(k_x/2) + \sin^2(k_y/2)) \cdot \boldsymbol{\sigma} \tag{7}$$

This yields a novel presentation and visualization of its full phase diagram. It also serves as a model with several chambers as those discussed in §3.4.3.

The function from $T^2 \to \mathbb{R}^3$ misses the origin if $M \neq 0, M \neq B, M \neq 2B$. The intersection with the z-axis is given by $k_x = 0, \pi; k_y = 0, \pi$. The images of these points are $(0,0) \mapsto (0,0,M), (0,\pi) \mapsto (0,0,M-B), (\pi,0) \mapsto (0,0,M-B), (\pi,\pi) \mapsto (0,0,M-2B)$. The indices can be computed as $\cos(k_x)\cos(k_y)$ which are $+1,-1,-1,+1$, respectively. There are 6 regions; taking into account how many of the 4 points above lie on the ray $\lambda(0,0,1), \lambda > 0$, we obtain Table 1. The corresponding phase diagram is shown in Fig. 3. It is a straightforward check that the wall transitions are minimal and of rose-type. For the specific parameter values of $M = B = 1$, the surface is shown in Fig. 2. This choice of parameter lies in the critical set, as the origin lies on the surface. Slightly increasing M and moving the surface up keeps $(0,0,M)$ on the positive z-ray, and moves the two points $(0,0,M-B)$ onto the positive part of the ray, yielding the Chern number -1 corresponding to region 2. Moving the surface slightly down by decreasing M only leaves the point $(0,0,M)$ on the positive z-ray, which yields the Chern number 1 corresponding to region 1. This can also be read off from Fig. 3 and Table 1.

Example 3.3. As an example of how to construct a model with an arbitrary Chern number, we can implement the strategy of using higher degree maps. In this way, we recover the following example of [44]. Starting from the particular tight-binding model given by $h(k_x, k_y) = (h_1, h_2, h_3)$

$$h_1(\mathbf{k}) = \alpha\cos(k_x), \quad h_2(\mathbf{k}) = \beta\cos(k_y), \quad h_3(\mathbf{k}) = m_0 + \gamma_1 \sin k_x + \gamma_2 \sin k_y \tag{8}$$

using the same type of analysis, and using the Heaviside θ function, the Chern classes depend on the parameters as follows:

$$\deg(\hat{\mathbf{h}}) = sign(\alpha\beta) \sum_{n=0}^{1}\sum_{m=0}^{1}(-1)^{m+n}\theta(m_0 + (-1)^n\gamma_1 + (-1)^m\gamma_2) \tag{9}$$

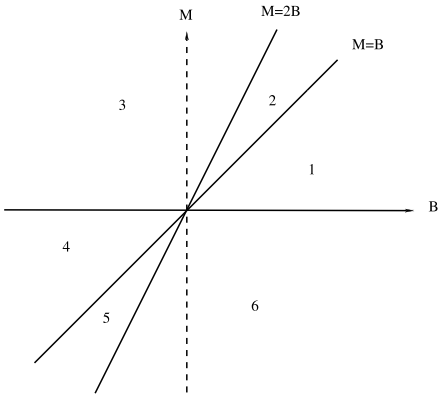

Fig. 3. Phase diagram corresponding to the phases listed in Table 1.

Table 1
Chern number of the open regions in the phase diagram of (7).

Region	Hyperplanes	Chern number
1	$B > M, M > 0$	1
2	$2B > M, M > B$	−1
3	$M > 0, M > 2B$	0
4	$0 > M, M > B$	−1
5	$M < B, M > 2B$	1
6	$M < 2B, M < 0$	0

This yields Chern classes in $\{0, \pm 1\}$. Precomposing with a higher-degree map $f_d : S^2 \to S^2$ corresponding to the map Sz^d, which in coordinates $\mathbb{R}^3 = \mathbb{C} \times \mathbb{R}$ is given by $(x + iy, z) \mapsto ((x + iy)^d, z)$, leads to the construction of a new Hamiltonian for $d \in \mathbb{Z}^+$:

$$\tilde{h}_1(\boldsymbol{k}) + i\tilde{h}_2(\boldsymbol{k}) = \left(\alpha \cos k_x - i\beta \cos k_y\right)^d, \quad \tilde{h}_3(\boldsymbol{k}) = m_0 + \gamma_1 \sin k_x + \gamma_2 \sin k_y \tag{10}$$

Here, $\alpha, \beta, \gamma_{1,2}$, and $m_0 \in \mathbb{R}$ are parameters. The resulting Hamiltonian will have Chern number d times the original Hamiltonian.

4. Lattice implementation

Here and in the following, we work in the usual physical setup, utilizing creation and annihilation operators to realize the hopping terms and other interactions, to facilitate the connection to the literature. In this framework, the translation from site i to site $i + m$ in a one-particle system is given by $U_m = c^\dagger_{i+m} c_j$. For instance in $\mathbb{Z}^2$ there are the operators $U_1 = c^\dagger_{i+1,j} c_{i,j}$ and $U_2 = c^\dagger_{i,j+1} c_{i,j}$.

For concrete condensed matter systems, we will achieve higher Chern numbers by using commensurate higher-order neighborhoods. These geometrically correspond to coverings (18). If the Hamiltonians already involve higher-order interactions as the Haldane Hamiltonian, see Example 4.4 below, we require that all the participating n–th neighborhoods are commensurate in the super-lattice, that is they are all scaled by the same integer $l(k)$. In particular, given a Hamiltonian with interaction terms $H^{(n)}$, under the condition that all these sublattices are commensurate, under multiplication by $l(k)$ the interaction terms will become $l(k)H^{(n)} = H^{(kn)}$.

4.1. Tight-binding lattice Hamiltonians

One standard setup is to consider a periodic Hamiltonian $H(x) = H(x + l)$ where $l \in \Lambda \subset \mathbb{R}^n$ is a translational lattice group $\Lambda \simeq \mathbb{Z}$, cf. e.g. [38]; we will call this the mathematical lattice. Using Fourier transform, in momentum space this yields a family of Hamiltonians $H(k)$ $k \in \mathbb{R}^n/\mathbb{Z}^n = T^n = (S^1)^{\times n}$. Here $\mathbb{Z}^n = \check{\Lambda}$ is the dual lattice for the standard inner product. The space is then discretized into a site lattice Γ—the physical lattice—, which is translationally invariant $l\Gamma = \Gamma$ for all $l \in \Lambda$. Γ is actually a graph, here embedded 1-d CW complex, which means that it also has edges. If only the vertices are given, then the edges are defined to connect nearest neighbors. The (periodic) elementary cell is $\bar{\Gamma} = \Gamma/\Lambda$, we denote by $\pi : \Gamma \to \bar{\Gamma}$ the projection, and let $d = |\bar{\Gamma}|$ be the number of sites in an elementary cell. The basic yet fundamental example of a Hamiltonian for this geometry is given by the standard Harper Hamiltonian. The Hilbert space is $\mathcal{H} = \ell^2(\Gamma)$, where $\ell^2(\Gamma)$ are the ℓ^2 (viz. square summable) functions on the set of vertices, and the Hamiltonian is given by translation along the edges. Practically, this is done by choosing a root vertex and setting E of generating directed edges. Concretely: let $\Gamma_v = \pi^{-1}(v)$, and split the Hilbert space as $\bigoplus_{v \in \bar{\Gamma}} \ell^2(\Gamma_v)$, the Hamiltonian becomes a $d \times d$ Hermitian family of matrices on momentum space: $H(k) : T^n \to Herm_d$, $H = \sum_{e \in E} U_e + U_e^\dagger$ where U_e are Zak

(magnetic) translation operators, see e.g. [3]. Note that, as defined, this is an operator-valued matrix. To have a "true" matrix, that is, an element in $End(\mathcal{H})$ of some Hilbert space, one needs to fix a spanning tree. There are several such choices that are related by re-gauging transformations, see [45].

Taking the perspective of this family of Hamiltonians over the Brillouin zone. The corresponding Bloch bundle is the trivial bundle $E = T^n \times \mathbb{C}^d \xrightarrow{\pi} T^n$, where $\pi = \pi_1$ is the projection to the first factor. Being trivial, this carries no information, but on the locus $T^n_0 \subset T^n$ where the Hamiltonians are non-degenerate, E splits as $\bigoplus_{i=1}^d L_i$ where L_i are the Eigenbundles to the Eigenvalues λ_i. Since the Eigenvalues are real and do not cross, we can order them $\lambda_1 < \lambda_2 \cdots < \lambda_d$. One can add different orbitals for more bands and on-site potentials for additional diagonal elements.

Example 4.1. For the $\mathbb{Z}^2$–lattice after Fourier transform, or equivalently applying a character $\chi : C^*(T^2) \to \mathbb{C}$ with $\chi(U) = e^{ia}, \chi(V) = e^{ib}$, the Harper Hamiltonian $H = U_{e_1} + U_{e_2} + U_{e_1}^\dagger + U_{e_2}^\dagger$ reads $H = e^{ia} + e^{-ia} + e^{ib} + e^{-ib} = 2(\cos a + \cos b) = 4\cos\left(\frac{a+b}{2}\right)\cos\left(\frac{a-b}{2}\right)$.

Example 4.2. For the hexagonal lattice, with generating vectors $a_1 = (0,-1), \quad a_2 = \left(\frac{\sqrt{3}}{2}, \frac{1}{2}\right), \quad a_3 = \left(-\frac{\sqrt{3}}{2}, \frac{1}{2}\right), \quad a_1 + a_2 + a_3 = 0$, moving from the A (blue) to the B (red) sites in Fig. 4(a), using $U = T_{a_1}, V = T_{a_2}$, and $W = T_{a_3} = (UV)^{-1}$: the Hamiltonian is

$$H_{hex} = \begin{pmatrix} 0 & U + V + W \\ U^\dagger + V^\dagger + W^\dagger & 0 \end{pmatrix} \tag{11}$$

Using a character $\chi(T_{a_j}) = e^{i\mathbf{k}\cdot a_j}$

$$H_{hex} = \begin{pmatrix} 0 & \sum_j e^{i\mathbf{k}\cdot a_j} \\ \sum_j e^{-i\mathbf{k}\cdot a_j} & 0 \end{pmatrix} = (\sum_j \cos(\mathbf{k}\cdot a_j))\sigma_x + (\sum_j \sin(\mathbf{k}\cdot a_j))\sigma_y \tag{12}$$

The family is degenerate at the Dirac points $K = \left(\frac{4\pi}{3\sqrt{3}}, 0\right)$ and $K' = \left(-\frac{4\pi}{3\sqrt{3}}, 0\right)$. It has no σ_z component and already for this reason, there will be no non-zero Chern class as discussed in [10, Section 4.11]. To get a non-trivial Chern number, following Haldane, one can invoke higher-order interactions, see the next paragraph.

4.1.1. *Higher neighborhood interactions*

One way to obtain new terms in the Hamiltonian that correspond to higher degree maps is to consider interactions that are next nearest or even further neighbors. The Hamiltonian will generally involve terms for all neighbors up to the dth neighbors. For the example of the square lattice (10) this was done in [44]. We will give a detailed analysis for several geometries in §5.1. Abstractly, the setup is the following. Consider a lattice $\Gamma \subset \mathbb{R}^n$ whose edges are generated by edge vectors $v_1, \dots, v_n$, and let the sublattice Γ^n of nth nearest neighbors have edges generated by the vectors $w_1, \dots w_k$. Expressing $w_i = \sum_j a_{ji} v_j$, the nth nearest neighbor hopping is then given by $H^{(n)} = \sum_i \prod_j U_j^{a_{ij}}$, where the U_j are the original translation operators along the v_j.

Example 4.3. In the square lattice $\mathbb{Z}^2$, the lattice vectors for the four 2nd nearest neighbors are $w_1 = (1,1), w_2 = (-1,1), w_3 = (-1,-1)$ and $w_4 = (-1,-1)$. These are at distance $\sqrt{2}$ and the Hamiltonian is $H^{(2)} = U_1U_2 + U_1U_2^* + U_1^*U_2^* + U_1^*U_2$. Transforming $V_1 = U_1U_2$ and $V_2 = U_1U_2^*$ we transform $H^{(2)}$ to the form H. This is the fact that the sublattice of second nearest neighbors is given by the sublattice $\mathbb{Z}(1,1)+\mathbb{Z}(1,-1) \subset \mathbb{Z}^2$. This is rotated by 45° and stretched by $\sqrt{2}$. There are again four 3rd nearest neighbors $(\pm 2, 0), (0, \pm 2)$ at distance 2 with Hamiltonian $H^{(3)} = U_1^2 + U_2^2 + U_1^{-2} + U_2^{-2}$. Rewriting $V_i = U_i^2$, we see that $H^{(3)}$ transforms into H. However, evaluating with a character, we have $V_1 = e^{2ia}, V_2 = e^{2ib}$, that is we get the pullback under $z \to z^2$. This expresses the fact that the sublattice of 3rd nearest neighbors is $(2\mathbb{Z})^2 \subset \mathbb{Z}^2$. The full systematic treatment is in §4.2.1, see in particular Table 2 and §4.3. This shows the sublattices of nearest neighbors which are multiples of $\mathbb{Z}^2$. After rotating by 45° and stretching by $\sqrt{2}$ we find a second series of nearest neighbors.

Example 4.4. The second-order interactions for the hexagonal lattice are diagonal, and the corresponding Hamiltonian is given by

$$H^{(2)}_{hex} = \begin{pmatrix} VW^* + WU^* + UV^* + h.c. & 0 \\ 0 & VW^* + WU^* + UV^* + h.c. \end{pmatrix} \tag{13}$$

Adding first and second order interactions with a coupling and applying the character, and setting $b_1 = a_2 - a_3, b_2 = a_3 - a_1, b_3 = a_1 - a_2$, we obtain'

$$\begin{aligned} H_{hex} + t_2 H^{(2)}_{hex} &= \begin{pmatrix} t_2(\sum_j e^{i\mathbf{k}\cdot b_j} + \sum_j e^{-i\mathbf{k}\cdot b_j}) & \sum_j e^{i\mathbf{k}\cdot a_j} \\ \sum_j e^{-i\mathbf{k}\cdot a_j} & t_2(\sum_j e^{i\mathbf{k}\cdot b_j} + \sum_j e^{-i\mathbf{k}\cdot b_j}) \end{pmatrix} \\ &= 2t_2(\sum_j cos(\mathbf{k}\cdot b_j))\sigma_0 + (\sum_j \cos(\mathbf{k}\cdot a_j))\sigma_x + (\sum_j \sin(\mathbf{k}\cdot a_j))\sigma_y \end{aligned} \tag{14}$$

Note that the families (13) and (14)—even on the non-degenerate locus—are pull-backs with mapping degree 0 as there are no σ_z terms and hence the map $h(\mathbf{k})$ is not surjective.. To alter this, one has to introduce an asymmetry in the coupling. First, one can introduce an asymmetric mass term $m\sigma_z$ and secondly, following Haldane [11], a complex coupling $e^{\pm i\phi}$ for the next nearest neighbor action, with a convention that ensures that the net magnetic flux through each unit cell is zero, see (see Fig. 4(a)). This

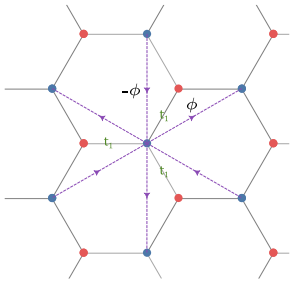

(A) Haldane model on a honeycomb lattice.

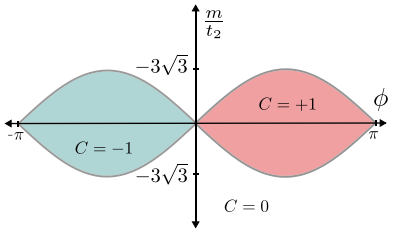

(B) A slice of the 3-parameter family of Hamiltonians with $t_2 = 1$ in the Haldane Hamiltonian Eq. (16).

Fig. 4. Topological Phases of the Haldane model on a honeycomb lattice.

breaks time-reversal symmetry, thus allowing for a non-zero Chern number. Mathematically, this avoids having a degree zero map by ensuring that the line bundle of the ground state is not isomorphic to its complex conjugate.

$$H^2_{\text{Hal}}(\phi) = \begin{pmatrix} e^{i\phi}(VW^* + WU^* + UV^*) + h.c. & 0 \\ 0 & e^{-i\phi}(VW^* + WU^* + UV^*) + h.c. \end{pmatrix} \tag{15}$$

The Hamiltonian family is then $H_{\text{Hal}} = H_{hex} + t_2 H^2_{\text{hal}}(\phi) + m\sigma_z$. To connect to the physics literature, using creation/annihilation operators on the A and B sublattices, The Hamiltonian is given by:

$$H = \sum_{\langle i,j\rangle} (c^\dagger_{i,A} c_{j,B} + c^\dagger_{i,B} c_{j,A}) + t_2 \sum_{\langle\langle i,j\rangle\rangle} (e^{\pm i\phi} c^\dagger_{i,A} c_{j,A} + e^{\mp i\phi} c^\dagger_{i,B} c_{j,B}) + m \sum_i (c^\dagger_{i,A} c_{i,A} - c^\dagger_{i,B} c_{i,B}) \tag{16}$$

After applying a character, we have $H_{\text{Hal}}(\mathbf{k}) = \sum_{i=0}^3 h_i(\mathbf{k})\sigma_i$ where

$$\begin{aligned} h_0(\mathbf{k}) &= 2t_2 \cos\phi \sum_{i=1}^3 \cos\left(\mathbf{k}\cdot b_i\right), \quad h_1(\mathbf{k}) = \sum_{i=1}^3 \cos\left(\mathbf{k}\cdot a_i\right) \\ h_2(\mathbf{k}) &= \sum_{i=1}^3 \sin\left(\mathbf{k}\cdot a_i\right), \quad h_3(\mathbf{k}) = m - 2t_2 \sin(\phi) \sum_{i=1}^3 \sin\left(\mathbf{k}\cdot b_i\right) \end{aligned} \tag{17}$$

This defines a 3-parameter family of Hamiltonians depending on real variables $\{t_2, \phi, m\}$. The vectors $\{a_i, b_i\}$ are the first and second-nearest neighbor vectors, respectively. After scaling the σ_0 term to 0 see Theorem 2.1, the Eigenvalue, aka. energy, spectrum is $E_\pm = \pm\sqrt{h_1^2 + h_2^2 + h_3^2}$. Looking along the ray given by $(0,0,1)$, we see that $h_1 = h_2 = 0$, which yields K and K' from above. The spectrum is only degenerate if $h_3 = 0$ also vanishes; then they again are Dirac points. This happens along the two curves: $m = \pm 3\sqrt{2}\, t_2 \sin\phi$. The positive branch $m = 3\sqrt{2}\, t_2 \sin\phi$ corresponds to crossing the origin at K (the negative branch is at K'). This gives the phase diagram, Fig. 4(b). Note that there is a direct transition from -1 to $+1$ along the ϕ axis, and, since this is 2–band system, by Theorem 3.1 there need to be at least two Dirac points. Indeed, there are exactly two of these points K and K' and this example is minimal. Moreover according to 3.4.2, the wall crossings are between Chern numbers $0, \pm 1$ which are modeled by the circle of §3.4.2 while the wall crossing -1 to 1 along the line $\frac{m}{t_2}$ is a collapse to the interval, see *loc. cit.*, where variables $\{i, j\}$ denote lattice site positions and the summations $\langle i, j\rangle$ and $\langle\langle i, j\rangle\rangle$ are over first and second-nearest neighbors, respectively.

4.1.2. Supercells

The way to geometrically understand how higher-order neighborhood interactions generate higher Chern classes is via supercells. A typical situation in condensed matter theory is given by covers coming from a sublattice in a lattice. Let $\Lambda' \subset \Lambda$ both be mathematical lattices of rank n —the standard example being $(2\mathbb{Z})^n \subset \mathbb{Z}^n$. Then the quotient map

$$\pi : T^n = \mathbb{R}^n/\Lambda' \to (\mathbb{R}^n/\Lambda)/(\Lambda/\Lambda') = \mathbb{R}^n/\Lambda' = T^n \tag{18}$$

is a degree $|\Lambda/\Lambda'|$ covering. We can now pull back a family from T^2 by π to obtain higher Chern classes on T^2. This corresponds to looking at a supercell, which covers the regular cell. In particular, using the volume form ω induced from the standard volume form on $\mathbb{R}^n$, we can compute the degree of the map π as $deg(\pi) = \frac{Vol(\mathbb{R}^n/\Lambda)}{Vol(\mathbb{R}^n/\Lambda')} = Vol(\Lambda/\Lambda')$. If one has a physical lattice Γ, then one has the two quotients $\bar\Gamma = \Gamma/\Lambda$ and $\bar\Gamma' = \Gamma/\Lambda'$ and a covering map $\pi_\Gamma : \bar\Gamma' \to \bar\Gamma$ which is a discrete cover of degree $d = |\Lambda/\Lambda'|$. The lattice $\bar\Gamma'$ lifts to a sublattice Γ' of Γ whose index $[\Gamma/\Gamma'] = d$. Note if $\Lambda' \subset \Lambda$ is a sublattice of the translational lattice, then for the duals, the reverse inclusion holds $\check\Lambda \subset \check\Lambda'$.

Example 4.5. The physical hexagonal lattice Γ_{hex} lies in the physical triangular lattice Γ_{tri}. The translational lattice $\Lambda_{hex} \subset \Lambda_{tri}$ is generated by $b_1 = a_1 + a_2, b_2 = 2a_2 - a_1$, if a_1, a_2 generate Λ_{tri}. Then $[\Lambda_{tri} : \Lambda_{hex}] = |\begin{vmatrix} 1 & 1 \\ -1 & 2 \end{vmatrix}| = 3 = [\check\Lambda_{hex} : \check\Lambda_{tri}] = deg(f)$ where $f : T^2 = \mathbb{R}^2/\Lambda_{tri} \to \mathbb{R}_2/\Lambda_{hex} = T^2$.

Definition 4.1. We call a sublattice of k–th nearest neighbors $\Gamma^k \subset \Gamma \subset \mathbb{R}^n$ *commensurate*, if $\Gamma^k = l(k)\Gamma$, where $l(k)$ is the distance of the nearest neighbors.

In this case the coefficients of $H^{(n)} = \sum_i \prod_j U_j^{a_{ij}}$ satisfy $a_{ij} = l(k)$, and the cover is of degree $l(k)^n$. The following is now straightforward:

Proposition 4.1. *For a commensurate k–th nearest neighbor lattice, the family of Hamiltonians $H^{(k)} : T^n \to Herm_d$ is the pull-back of the original lattice Hamiltonian under the diagonal scaling map $f_{l(k),\dots,l(k)} : T^n \to T^n : (\theta_1, \dots, \theta_n) \mapsto l(k)(\theta_1, \dots, \theta_n) = (l(k)\theta_1, \dots, l(k)\theta_n)$ whose degree is $l(k)^n$. Hence, all Chern classes of the original family are scaled by $l(k)^n$.* □

Remark 4.1. Thus, the question of finding natural lattice implementations turns into the question of finding commensurate higher-order neighborhoods. For a large family of 2D–lattices, this is done in §5.1. Unraveling the definitions, this means that if the original Hamiltonians were of the form $H(k_x, k_y) = f(k_x, k_y) \cdot \boldsymbol{\sigma}$, then the Hamiltonian belonging the commensurate sublattice with $l(k) = N$ is $H^{[C=N^2]} = f(Nk_x, Nk_y)$, see §5.1 for examples.

In the more general case of $H^{(n)} = \sum_i \prod_j U_j^{a_{ij}}$, with the $a_{ij} \in \mathbb{N}$ we can evaluate with a character $\chi : U_j \to e^{i\theta_j}$ and then $U_j^{a_{ij}} \mapsto e^{ia_{ij}\theta_j}$, but if there are $a_{i,j} \neq 0$ for $i \neq j$, this transformation not a simple rescaling of the angles in the matrix coefficients. A multi-rescaling $a_{ij} = 0, i \neq j$ does do this simple rescaling with several stretching factors, setting $d_i = a_{ii}$, the pull-back map is $f_{d_1,\dots,d_n}(\theta_1, \dots, \theta_n) = (d_1\theta_1, \dots, d_n\theta_n)$. It is clear, though, that the lattice spanned by $d_i v_i$ can only be a nearest neighbor lattice if $d_i \equiv d$ is constant. The second best thing is if there is a base-change, that is an operation of $SL(n, \mathbb{Z})$ and a homothety which results in a sublattice of nearest neighbors. This is possible, but even harder to classify. We can do this for the case of a square lattice, see also Example 4.6, and for the triangular lattice, see §4.3.

We stress that all these sublattices, base-change followed by stretching, exist and present valid Hamiltonians. These do not satisfy simple physical interpretations. For these, we restrict to n–the nearest neighbors. The commensurate lattices are singled out for simplicity of formulas and for possible applications as they afford the tightest control.

4.1.3. Band structures for sublattices

In this section, we analyze the effect of larger Brillouin zones, e.g. those coming from stacking. For a sublattice and a lattice, the matrix dimension of the two families of Harper, tight-binding Hamiltonians differs by $|\Lambda/\Lambda'| = \frac{d'}{d}$, where $|\Gamma/\Lambda'| = d'$ and $|\Gamma/\Lambda| = d$. To compare the two, one should re-sum the larger block–Hilbert spaces as

$$\mathcal{H}_{\tilde{\Gamma}'} = \bigoplus_{v \in \tilde{\Gamma}'} \ell^2(\Gamma_v) \simeq \bigoplus_{w \in \tilde{\Gamma}} \Big(\bigoplus_{v \in \pi_\Gamma^{-1}} \Gamma_w \Big) \tag{19}$$

This amounts to summing the entries given after the application of the translation operators.

Example 4.6. As an example on $\Lambda = \mathbb{Z}^n$, we have the 1×1 Harper Hamiltonian $H = \sum_{i=1}^n U_i + U_i^\dagger$. For the sublattice $\Lambda' = (2\mathbb{Z})^2 \subset \mathbb{Z}^2$ of index 4 the operator is the Harper Hamiltonian derived for the lattice $2\mathbb{Z}^2$ is given by a 4×4 matrix $H_4 = \tilde{U}_1 + \tilde{U}_1^\dagger + \tilde{U}_2 + \tilde{U}_2^\dagger$, where the operators $\tilde{U}_1$ and $\tilde{U}_2$ are

$$\tilde{U}_1 = \begin{pmatrix} 0 & 0 & 0 & W_1 \\ 0 & 0 & W_3^\dagger & 0 \\ 0 & W_3 & 0 & 0 \\ W_1^\dagger & 0 & 0 & 0 \end{pmatrix} \quad \tilde{U}_2 = \begin{pmatrix} 0 & 0 & W_2 & 0 \\ 0 & 0 & 0 & W_4^\dagger \\ W_2^\dagger & 0 & 0 & 0 \\ 0 & W_4 & 0 & 0 \end{pmatrix} \tag{20}$$

with the W_i representing the translations along the edges in the new, bigger, unit cell. The original bundle embeds under the diagonal map on the fibers $\Delta^{[4]} : \mathbb{C} \to \mathbb{C}^4$. In particular, $H_4(1,1,1,1)^T = H_1(1,1,1,1)$ where H_4 and H_1 are the 4×4 and the 1×1 families, respectively. Note that in C^* geometry, see e.g. [3,46], the entries are from the 4-torus and the corresponding map $T^2 \to T^4$ along which the family restricts to is given by $W_1, W_3 \to U_1$ and $W_2, W_4 \to U_2$ on generators. This corresponds to the fact that the respective spatial translations are along the same vector.

If one would simply start with the quotient graph $\mathbb{Z}^2/(2\mathbb{Z})^2$, Then, abstractly, one would have the more general Hamiltonian

$$\hat{H}_4 = \begin{pmatrix} 0 & 0 & V_2 + V_6^\dagger & V_1 + V_5^\dagger \\ 0 & 0 & V_3^\dagger + V_7 & V_4^\dagger + V_8 \\ V_2^\dagger + V_6 & V_3 + V_7^\dagger & 0 & 0 \\ V_1^\dagger + V_5 & V_4 + V_8^\dagger & 0 & 0 \end{pmatrix} \tag{21}$$

This more general Hamiltonian has more operators and hence parameters. These can stand for more sites resulting from stacking or more orbitals. The specialization equations that turn $\hat{H}_4$ into H_1 are given by $V_1 = V_3 = V_5 = V_7 = U_1$ and $V_2 = V_4 = V_6 = V_8 = U_2$, which corresponds to the iterated diagonal embedding $T^2 \to T^4 \to T^8$. This again reflects that the translations in physical space are along the same vectors.

4.1.4. Band folding

There is, more generally, the possibility of pushing forward a family of Hamiltonians. This has the effect of what is known as band-folding. Given a family of Hamiltonians $H : B' \to Herm_d$ and a covering $\pi : B' = \mathbb{R}^n/\Lambda' \to B = \mathbb{R}^n/\Lambda$ with $\Lambda' \subset \Lambda$, for $\mathbf{v} \in \Lambda/\Lambda'$ consider the translation operator $T_\mathbf{v} : \mathbb{R}^n/\Lambda' \to \mathbb{R}^n/\Lambda' : T_\mathbf{v}([l]) = [l + \mathbf{v}]$. Fix one section s_0 of π and set $s_\mathbf{v} = T_\mathbf{v} s_0$, i.e. the section obtained by shifting by the action of translation by $\mathbf{v}$. Now consider $\phi_*(V) = \bigoplus_{\mathbf{v}\in\Lambda/\Lambda'} s_\mathbf{v}^* V$. The corresponding push-forward Hamiltonian in momentum space is given as follows: $\pi_*(H) = \bigoplus_{\mathbf{v}\in\Lambda/\Lambda'} T_\mathbf{v}(H)$, i.e. $\pi_*(H)(\mathbf{k}) = \bigoplus_{\mathbf{v}\in\Lambda/\Lambda'} H(\mathbf{k}+\mathbf{v})$. This also has the effect of increasing the size of the matrix by a factor Λ/Λ'. The problem of unfolding is identifying the original band structure in the pull-back of the push-forward, $\pi^*\pi_*(H)$.

4.1.5. Designing lattice Hamiltonians

We can also read the known lattice constructions backwards to design specific lattice local Hamiltonians. For instance, to get a version of the Chern-number ± 1 from the continuum Hamiltonian $\mathbf{k}\cdot\boldsymbol{\sigma}$ for a lattice, we first need a 2-band system. The choices are either a lattice with two sublattices, like the hexagonal lattice, or, if we stick to a square lattice, we use a stacking of two orbitals to have the $H(\mathbf{k})$ in $Herm_2$. As a 2-band system, after shifting the system to be traceless, we can always write these as $H(\mathbf{k}) = f(\mathbf{k})\cdot\boldsymbol{\sigma}$. Then the Chern number realized depends on the mapping degree of $f(\mathbf{k})$. For the mapping degree to be non-zero, we need $f(\mathbf{k})$ to be at least surjective. This is why the first neighbor hopping on the hexagonal lattice does not suffice to produce a non-zero Chern number. There is no z-component of f, so it is not surjective. We can try to add that by going to second nearest neighbors in the hexagonal lattice; this is not a traceless term, but rather propositional to σ_0 due to the symmetry, but adding an asymmetry, namely ϕ, makes the function surjective, see Eq. (15). This deconstruction *a posteriori* explains Haldane's insight [11].

As a method, to design a system with a given phase diagram, one can find a solution of the form $f(\mathbf{k})\cdot\boldsymbol{\sigma}$ for possibly general spin and then in a second step create a realization in terms of a lattice. Here one first picks the number of bands and then realizes them as sublattices in a larger lattice, as orbitals, by stacking or a combination of these. For the lattice part, the most obvious terms that are available are the hopping or neighbor interactions, which is why we have concentrated on these. The classification Theorem 4.1 tells us what kind of terms with what kind of Chern numbers are readily available in integer quadratic lattices and those based on them, cf. §5.1.7, 5.1.10 and 6.

Finally, one can expand the matrices and control that they can be written in terms of spin matrices, so that one can compute their Chern numbers as mapping degrees. A tool to ensure this comes from using projectors to the spin components. For instance, the Haldane system in 1d [30,47] was designed by tensoring two spin-$\frac{1}{2}$ neighbors and then projecting to the spin-1 component. Similar implementations are possible on different lattices, which, however, exhibit distinct geometries.

4.2. Quadratic integer lattices

Two-dimensional lattices described by rings of quadratic integers provide a rich source of tight-binding models generalizing the square and triangular lattices. They are of the form $\mathbb{Z}[\omega] = \{a + \omega b \mid a, b \in \mathbb{Z}\}$, with $\omega = \frac{1+\sqrt{-d}}{2}$ when $-d \equiv 1 \pmod 4$ and $\omega = \sqrt{-d}$ otherwise. As we show in Appendix A, they provide infinite families of commensurate sublattices that furnish systematic ways to realize higher Chern numbers and more complex phase diagrams. The main tool we use is the norm function. After embedding into $\mathbb{C}$ by identifying $\sqrt{-d} = i\sqrt{d}$, the norm of an element is simply its complex absolute value, cf. §A.1.

A unit in a quadratic integer ring is an invertible element. Units are precisely those elements whose norm equals 1. An associate μ of an element $\nu \in \mathbb{Z}[\omega]$ is a quadratic integer that satisfies $\nu = u\cdot\mu$ for some unit u. The set of all associates of a given element is finite in $\mathbb{Z}[\omega]$, cf. [48]. In fact, the number of units $|U|$ is 2, 4, or 6 depending on d, see (43). Since the norm is multiplicative, all associates share the same norm.

Definition 4.2. An element $\mu \in \mathbb{Z}[\omega]$ is said to have an isolated norm if all the elements with the same norm as μ are associates. In other words, the lattice points whose distance squared from the origin is equal to that norm are unique up to lattice symmetry.

Up to a possible rotation, the elements whose norm is isolated span a sublattice which is a homothety of the original lattice by the square root of the norm. From A.1 and Theorems A.4 and A.3, using the definitions of split, ramified, and inert primes in §A.1, we obtain:

Theorem 4.1. *In a full 2D lattice Γ described by a quadratic integer ring $\mathbb{Z}[\omega]$, there are exactly $|U|$ nearest neighbors, U defined by (43), to any lattice point lying at a Euclidean distance $d = \prod_{i=1}^{r} p_i^{b_i} \prod_{j=1}^{s} q_j^{c_j/2}$ where each p_i is an inert prime $p_i \in \mathbb{Z}$ in $\mathbb{Z}[\omega]$, and $q_j \in \mathbb{N}$ is a ramified prime represented by the norm function, $b_i, c_j, r, s \in \mathbb{N}$, and $|U|$ is the cardinality of the set of units in $\mathbb{Z}[\omega]$. In particular, if $d \in \{-1, -2, -3, -7, -11, -19, -43, -67, -163\}$ then the domain is a unique factorization domain (UFD), and any ramified prime is represented, and the elements with these norms generate exactly those lattices with the same minimal number of nearest neighbors as the original lattice.* □

Remark 4.2. The role of UFD is the following: while Theorem 4.1 necessarily yields an infinite set of isolated norms, it is exhaustive only in UFDs. A counterexample in $\mathbb{Z}[\sqrt{-14}]$ is 3,5, which are split primes, but they have isolated norms. Moreover, in non-UFDs, it can happen that the product of two isolated norms is not an isolated norm. For example, consider the product $3\cdot 5$ again. Each factor has an isolated norm as can be checked explicitly; however, the numbers $1 \pm 4\sqrt{-14}$ and $13 \pm 2\sqrt{-14}$ are non-associates and also have the same norm as 15. This cannot happen in a UFD (as discussed later). Evidently, $\mathbb{Z}[\sqrt{-14}]$ has a class number of 4 and is thus a non-UFD. Another example in a domain with a class number of 3 is found in $Z[\frac{1+\sqrt{-23}}{2}]$. The two numbers 2,3 with isolated norms 4,9 multiply to give a number with a non-isolated norm.

We now illustrate this by treating topological insulators living on a square lattice ($d = -1$), and the triangular lattice ($d = -3$).

4.2.1. Gaussian integers/square lattice

Gaussian integers are the quadratic integers : $\mathbb{Z}[i] = \{a+bi : a, b \in \mathbb{Z}\}$. They form a square lattice in the complex plane and are a unique factorization domain (UFD) [49]. The norm of a Gaussian integer is $N(a+b\omega) = a^2+b^2$. There are four units $\{\pm 1, \pm i\}$ that have unit norm. The question of which norms are isolated in a quadratic domain boils down to the problem of finding a representation of integers as a certain quadratic form. In the case of Gaussian integers, non-isolated norms have a representation as the sum of two nonzero squares. This is a relatively old problem that was considered by Fermat. Many proofs for the theorem were given [49–51]. The results of Appendix A.3 can be used as a proof when specializing to Gaussian integers. Using Theorems A.1 and A.2, the only rational prime that ramifies (i.e. divides the discriminant $D = 4$) in $\mathbb{Z}[i]$ is $p = 2$. The primes of the form $p \equiv 3 \pmod 4$ remain inert while those of the form $p \equiv 1 \pmod 4$ split. A direct application of Theorem 4.1 in the case of Gaussian integers gives the following theorem.

Theorem 4.2 (*Fermat's theorem on sums of two squares*)**.** *An odd rational prime p can be represented as a sum of two nonzero squares $p = a^2 + b^2$ for $a, b \in \mathbb{N}$ iff $p \equiv 1 \pmod 4$.*

Restating this in terms of the distances of nearest neighbors in a square lattice, we have the following corollary.

Corollary 4.1. *In a square lattice, there are exactly four nearest neighbors to any lattice point at a Euclidean distance $d = 2^{b_0/2}\prod_{i=1}^{r} p_i^{b_i}$, with positive integers $r, b_i \in \mathbb{N}$, and each p_i is a rational inert prime, i.e. $p_i \equiv 3 \pmod 4$.*

Note that we will, in fact, restrict to the case where b_0 is an even integer. The parity of the number b_0 then divides this family of isolated norms into two classes whose lattice points are rotated from each other with an angle 45°; see Fig. 5(a) for an illustration of the first few isolated norms. For commensurate lattices, we take the parity of b_0 to be even, which yields distances: $d \in \{1, 2, 3, 4, 6, 7, 8, 9, 11, 12, 14 \cdots\}$.

4.2.2. Eisenstein integers/triangular lattice

Eisenstein integers are the quadratic integers: $\mathbb{Z}[\omega] = \{a + b\omega : a, b \in \mathbb{Z}\}$ where $\omega = e^{\frac{2\pi i}{3}} = -\frac{1}{2} - \frac{\sqrt{3}}{2}i$ is the cubic root of unity satisfying $1 + \omega + \omega^2 = 0$. Importantly, Eisenstein integers form a unique factorization domain (UFD) [49]. As an Abelian group, they form a triangular lattice in the complex plane. The norm of an Eisenstein integer is $N(a + b\omega) = a^2 + b^2 - ab$. There are six units $\{\pm 1, \pm\omega, \pm\omega^2\}$ that have unit norm. Moreover, $\mathbb{Z}[\omega]$ is an Euclidean domain where irreducible elements are primes [49]. By Theorems A.1 and A.2, a rational prime will ramify if it divides the field discriminant, which is -3. Consequently, the only rational prime that ramifies is $p = 3$. Furthermore, for primes other than 3, if $p \equiv 2 \pmod 3$ it remains inert, otherwise it splits. We have the following direct application of Theorem 4.1.

Corollary 4.2. *In a triangular lattice, there exist exactly six nearest neighbors to any lattice point at a Euclidean distance $d = 3^{b_0/2}\prod_{i=1}^{r} p_i^{b_i}$, for positive integers $r, b_i \in \mathbb{N}$, and each p_i is a rational inert prime $p_i \equiv 2 \pmod 3$.*

Note that, similar to the Gaussian integers case, the parity of the number b_0 then divides this family of isolated norms into two classes whose lattice points are rotated from each other with an angle 30°; see Fig. 5(b) for an illustration of the first few isolated norms. Thus, to obtain a commensurate sublattice, we will restrict to the case where b_0 is an even integer in the above corollary, which yields commensurate lattices at distances: $d \in \{1, 2, 3, 4, 5, 6, 8, 9, 10, 11, 12, 15, \ldots\}$.

4.3. Summary of lattice structure

In this short section, we summarize the results of the two important lattices of the previous section (the triangular lattice and the square lattice) where the proofs and generalizations are deferred to Appendix A. Assume that we have a lattice that supports an interaction between the N_0th-nearest neighbors. These neighbors are at a distance d_0 from the origin and at certain angles (denote their set of angles by $\Theta(d_0)$). More importantly, denote the number of these neighbors by $n(d_0)$. The gist of the previous section is that for certain new distances $d = Nd_0$ where $N \in \mathbb{N}$, the structure of the neighbors will be preserved. That is, the new nearest neighbors at the new distance d will have the same number ($n(d) = n(d_0)$) as those at distance d_0 and also the same angles ($\Theta(d) = \Theta(d_0)$).

Additionally, for the square lattice, we can multiply any of these allowed distances by $\sqrt{2}$, and we will get the same properties for the number of neighbors, but the angles will be rotated by 45°. For the triangular lattice, a similar story holds where multiplying the distance by $\sqrt{3}$ rotates the neighbors by 30°.

These allowed distances enable us to define lattice models with higher Chern numbers and, thus, a higher number of edge states, as we discuss in the next section. For convenience, the following table summarizes the first few allowed distances along with their nearest-neighbor hopping terms.

These allowed distances obey a simple rule are any product of the inert and ramified primes of their respective lattices. The rules for which primes ramify or stay inert follow from modulus properties as discussed in §4.2.1 and §4.2.2. Only split primes break the structure. These two lattices are important as they are ubiquitous for physical models. In addition, several other lattices, like honeycomb or Kagome lattices, are subsets of them, as we will expand on in the following section (see Table 3).

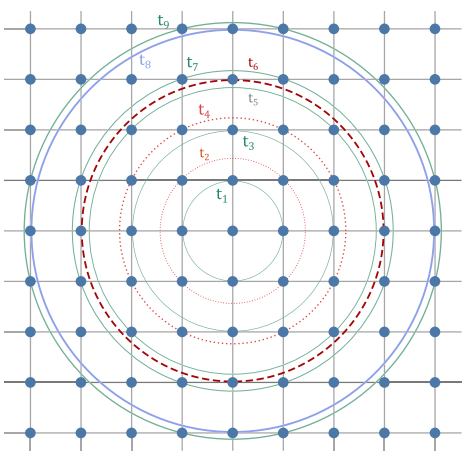

(A) The structure of the nearest-neighbor interactions in a square lattice. The 3rd, 6th, and 8th nearest neighbors form the sublattice $(d\mathbb{Z})^2$ with $d = 2, 3, 4$. They can be used to construct models with Chern numbers multiplied by $C = 4, 9, 16$, respectively.

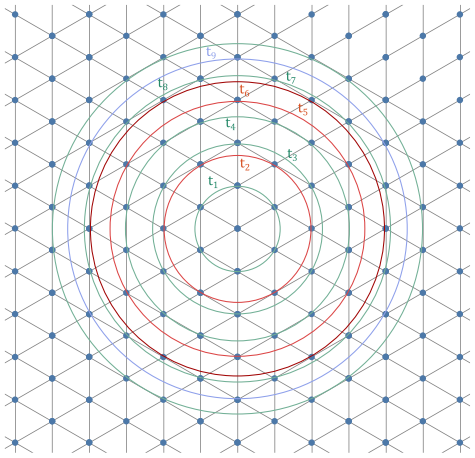

(B) The structure of distant neighbors in a triangular lattice. The number and orientation of nearest neighbors vary with distance. At distances $d \in \{1, 2, 3, 4\}$ we have commensurate lattices of 1st, 3rd, 6th and 9th nearest neighbors.

Fig. 5. Commensurate sublattices for the square and triangular lattices.

Table 2
First few allowed distances and hopping terms for square and triangular lattices.

Lattice	Allowed distances	Hopping terms
Square Lattice	$1, 2, 3, 4, 6, 7, 8, 9, 11, 12, 14$	$t_1, t_3, t_6, t_9, t_{13}, t_{18}$
Square Lattice (rotated 45°)	$\sqrt{2} \times 1, 2, 3, 4, 6, 7, 8, 9, 11, 12, 14$	$t_2, t_5, t_{11}, t_{16}, t_{24}$
Triangular Lattice	$1, 2, 3, 4, 5, 6, 8, 9, 10, 11, 12, 15$	$t_1, t_3, t_5, t_8, t_{11}, t_{15}$
Triangular Lattice (rotated 30°)	$\sqrt{3} \times 1, 2, 3, 4, 5, 6, 8, 9, 10, 11, 12, 15$	t_2, t_6, t_{12}, t_{19}

Table 3
First few primes classifications for square and triangular lattices.

Lattice	Ramified prime(s)	Inert primes	Split primes
Square Lattice	2	3, 7, 11, 19, 23	5, 13, 17, 29
Triangular Lattice	3	2, 5, 11, 17, 23, 29	7, 13, 19

5. Condensed matter model implementations

We now implement our strategy for natural models with higher Chern numbers for square and triangular lattices, which are quadratic integer lattices. Subsequently, we will treat the honeycomb and Kagome lattices, which are triangular-based lattices. By triangular-based, we mean lattices that are subsets of a triangular lattice, as discussed. These examples show how the construction can be easily extended to other lattices, such as Lieb, Dice, and checkerboard lattices.

5.1. Physical models with higher chern numbers $|C| > 1$

In this section, using concrete examples, we show how one can indeed achieve higher Chern numbers by using commensurate higher neighborhood interactions as discussed in §4.1.2 using the classification of commensurate lattices given above in 4.1.

The two main physical examples are the square and triangular lattices, as well as those based upon them, like the hexagonal and Kagome lattices. Building a Hamiltonian with couplings that include higher-order terms gives us access to phase transitions between topological phases with arbitrarily high Chern numbers.

5.1.1. Stacked square lattice

A simple Hamiltonian that realizes a Chern insulator on a square lattice was introduced in [16]. The model lives on a square lattice, but now with two orbitals per atom. This is the same as stacking two $\mathbb{Z}^2$ lattices on top of each other. This can also be thought of as a specific model for the index 2 sublattice $2\mathbb{Z} \oplus \mathbb{Z} \subset \mathbb{Z}^2$ which has two sites per unit cell, cf. Example 4.6, with extra

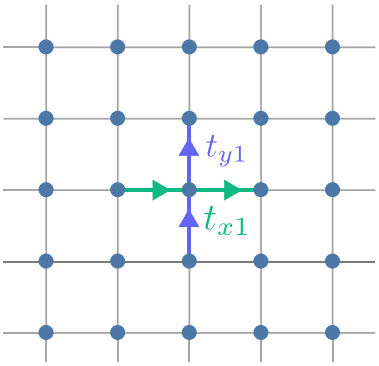

(A) A model for a topological insulator on a square lattice Eq. (22). Each atom has two orbitals, so the interaction terms t_{x1} and t_{y1} are 2×2 Hermitian matrices.

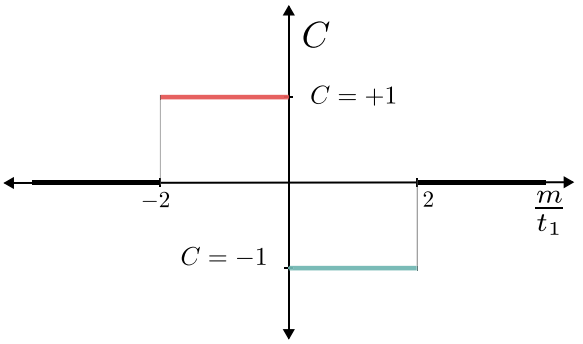

(B) One-dimensional phase diagram of the model for square lattice Eq. (22). The model is gapless for $\frac{m}{t_1}\in\{0,\pm 2\}$, otherwise it is gapped.

Fig. 6. Phases for the stacked square lattice.

anti-diagonal interaction terms. This also corresponds to having alternating short and regular distances along the x–axis. The Hilbert space again splits as $\mathcal{H}_A\oplus\mathcal{H}_B$—$A$ and B indicating the two orbitals. It represents the topological insulator mercury-telluride when we restrict to spin-up electrons [16,52]. The Hamiltonian using creation and annihilation operators reads:

$$\begin{aligned}H=-\frac{t}{2}\sum_i\Big\{&\left[c^\dagger_{i,A}\,c_{A,i+\hat{x}}-i\,c^\dagger_{i,A}\,c_{B,i+\hat{x}}-i\,c^\dagger_{i,B}\,c_{A,i+\hat{x}}-c^\dagger_{i,B}\,c_{B,i+\hat{x}}\right]\\&+\left[c^\dagger_{i,A}\,c_{A,i+\hat{y}}-c^\dagger_{i,A}\,c_{B,i+\hat{y}}+c^\dagger_{i,B}\,c_{A,i+\hat{y}}-c^\dagger_{i,B}\,c_{B,i+\hat{y}}\right]+\text{h.c.}\Big\}+m\sum_i\left[c^\dagger_{i,A}\,c_{i,A}-c^\dagger_{i,B}\,c_{i,B}\right].\end{aligned}$$

The two corresponding translation matrices are: $t_{x1}=(\sigma_z-i\sigma_x)\otimes T_{a_1}$ and $t_{y1}=(\sigma_z-i\sigma_y)\otimes T_{b_1}$, were a_1 and b_1 are the displacement vector to the nearest neighbor in the positive x and y direction.

The model is shown in Fig. 6(a). After Fourier transform, the Hamiltonian reads $H(\mathbf{k})=h(\mathbf{k})\cdot\sigma$ with

$$h_1(\mathbf{k})=t_1\sin(\mathbf{k}\cdot a_1),h_2(\mathbf{k})=t_1\sin(\mathbf{k}\cdot b_1),\quad h_3(\mathbf{k})=m-t_1\cos(\mathbf{k}\cdot a_1)-t_1\cos(\mathbf{k}\cdot b_1).\tag{22}$$

The ground state of the model with $\frac{m}{t}=-1$ has Chern number one, cf. [52]. The phase diagram was calculated using direct integration, and validated also through the ray method §2.1.5, and it is presented in Fig. 6(b).

5.1.2. Criteria for choosing distant neighbors in a square lattice

Identifying the lattice with the Gaussian integers $\mathbb{Z}+i\mathbb{Z}\subset\mathbb{C}$, see §4.2.1, we have commensurate nearest neighbors at distances specified in Corollary 4.1 with even b_0, that is $N\in\{2,3,4,6,7,8,9,11,\dots\}$. By tuning the range of hopping to any of the distances, corresponding to commensurate sublattices, we obtain a model with Chern numbers N^2 times the original ones. Indeed, moving to the commensurate sub–lattice of distance N neighbors effectively implements the mapping $f_{N,N}:T^2\to T^2,(\theta_1,\theta_2)\mapsto(N\theta_1,N\theta_2)$ whose degree is N^2, c.f. §2.1.6. The general form of Hamiltonian with Chern number N^2 is $H^{[C=N^2]}=h^{[C=N^2]}(\mathbf{k})\cdot\sigma$ with:

$$\begin{aligned}&h_1^{[C=N^2]}(k)=\sin(k\cdot Na_1)=\sin(Nk\cdot a_1),\quad h_2^{[C=N^2]}(k)=\sin(k\cdot Nb_1)=\sin(Nk\cdot b_1),\\&h_3^{[C=N^2]}(k)=\frac{m}{t_N}-\cos(k\cdot Na_1)-\cos(k\cdot Nb_1)=m-\cos(Nk\cdot a_1)-\cos(Nk\cdot b_1).\end{aligned}\tag{23}$$

Including terms for a subset $S\subset\{1,2,3,4,6,7,8,9,11,\dots\}$ of the commensurate distances with coupling coefficients, i.e. $H=\sum_{N\in S}t_N H^{[C=N^2]}$, we obtain a family which will have Chern numbers $\pm N^2$ and transitions between these Chern numbers.

5.1.3. Stacked triangular lattice

The next fundamental example is the case of a stacked triangular lattice realizing a Chern insulator on a triangular lattice [18]. The Hilbert space is again $\mathcal{H}_A\oplus\mathcal{H}_B$. It has an on-site potential m, real nearest-neighbor interaction switching the orbitals and a complex next-nearest-neighbor interaction keeping the orbitals, but with a phase $e^{\pm i\phi}$ chosen similar to Haldane's choice, cf. Fig. 7(a). Note that the second nearest neighbors are a rotated six-site lattice. The Hamiltonian reads

$$H=-t_1\sum_{\langle i,j\rangle}c^\dagger_{i,A}c_{j,B}-t_2\sum_{\langle\langle i,j\rangle\rangle}e^{i\phi_{ij}}\left(c^\dagger_{i,A}c_{j,A}+c^\dagger_{i,B}c_{j,B}\right)+m\sum_i\left(c^\dagger_{i,A}c_{i,A}-c^\dagger_{i,B}c_{i,B}\right)\tag{24}$$

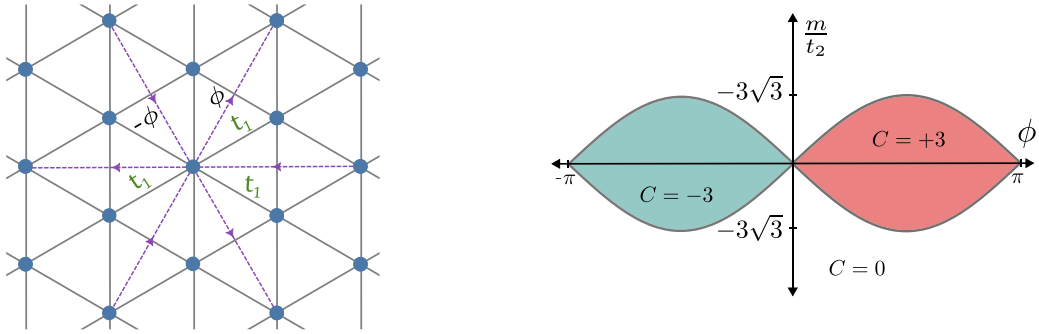

(A) Simple model for a Chern insulator on a triangular lattice. The phase ϕ is positive if it is aligned with the arrows and it is from A to B orbitals. Flipping the arrow or the order of the orbitals flips the sign of ϕ.

(B) Phase diagram of a modified Haldane model on a triangular lattice with $t_1 = 1$ in Eq. (25). The Chern number takes higher values {-3,3} as it is 3 times that of the Honeycomb lattice; compare with Fig. 4b.

Fig. 7. Hamiltonian terms patterns (left) and phase diagram (right) of a Chern insulator on a triangular lattice.

After making the model traceless, in momentum space the model reads $H(k) = h(k) \cdot \sigma$ with:

$$\begin{aligned} h_1(k) &= -\frac{1}{2}t_1 \sum_{i=1}^{6} \cos\Big(k \cdot a_i\Big), \quad h_2(k) = -\frac{1}{2}t_1 \sum_{i=1}^{6} (-1)^i \sin\Big(k \cdot a_i\Big) \\ h_3(k) &= m - t_2 \sin(\phi) \sum_{i=1}^{6} (-1)^i \sin\Big(k \cdot b_i\Big) \end{aligned} \tag{25}$$

Here, a_i and b_i denote the first and second-nearest neighbor vectors. This connection can be seen by noting that three stacked honeycomb lattices with one orbital per site are equivalent to a triangular lattice with two orbitals per site [18]. This equivalence results in Chern number $C = 3$ of the ground state [18], which is three times that of the same parameters in the Haldane model; see Fig. 4(b). An alternative way to compute this is to realize that a_i and b_i are symmetric, i.e the six vectors can be written as $\pm a_1, \pm a_2, \pm a_3$ resp. $\pm b_1, \pm b_2, \pm b_3$. Due to the symmetry of the sine and cosine, they give a factor 2 in the terms of the h_i, retaining only sums $i = 1, 2, 3$, this reads like the Haldane Hamiltonian (17). The factor of three comes from the inclusion of the dual triangular into the dual Hexagon lattice, which is of degree 3, see §2.1.5, The phase diagram was calculated using direct integration, and validated also through the ray method §2.1.5, and is then shown in Fig. 7(b).

Given this base Hamiltonian, we can construct a new Hamiltonian with a distant hopping that realizes a higher Chern number as follows:

$$\begin{aligned} h_1^{[C=N^2]}(k) &= -\frac{1}{2}t_1 \sum_{i=1}^{6} \cos\Big(Nk \cdot a_i\Big), \quad h_2^{[C=N^2]}(k) = -\frac{1}{2}t_1 \sum_{i=1}^{6} (-1)^i \sin\Big(Nk \cdot a_i\Big), \\ h_3^{[C=N^2]}(k) &= m - t_2 \sum_{i=1}^{6} (-1)^i \sin\Big(Nk \cdot b_i\Big). \end{aligned} \tag{26}$$

As before, the distant neighbors effectively implement the mapping $f_{N,N} : T^2 \to T^2, (\theta_1, \theta_2) \mapsto (N\theta_1, N\theta_2)$ whose degree is N^2 and the resulting Hamiltonian has a Chern numbers multiplied by $C = 0, \pm 3N^2$ since we started with a Hamiltonian with $C = 0, \pm 3$ §2.1.6. The wall crossings are from 0 to ± 3 given by circles, but now the origin is crossed 3 times, which leaves three pre-Dirac points after crossing to either of the two phases with a non-zero Chern number.

5.1.4. A second basic model for triangular lattices

We also note that in triangular lattices, we do not need to preserve the whole structure of the original Hamiltonian. We can also construct models that only preserve the structure of the t_1–coupled interaction terms, involving the off-diagonal terms stemming from σ_x and s_y while keeping the diagonal t_2–coupled terms stemming from σ_z the same. Such models should be of practical value as the complex interactions t_1 are harder to implement experimentally. These models do not arise as a pre-composition with a higher degree map, but rather as a post-composition with the map $z \to z^N, t \to t : S^2 \to S^2$, see §2.1.5. The new Chern number will be N

times the original one.

$$h_1^{[C=N]}(k) = -\frac{1}{2}t_1\sum_{i=1}^{6}\cos\Big(Nk\cdot a_i\Big),\quad h_2^{[C=N]}(k) = -\frac{1}{2}t_1\sum_{i=1}^{6}(-1)^i\sin\Big(Nk\cdot a_i\Big),$$
$$h_3^{[C=N]}(k) = m - t_2\sum_{i=1}^{6}(-1)^i\sin\Big(k\cdot b_i\Big). \tag{27}$$

One way to see this is to realize that $z = h_1 + ih_2 = e^{\imath\sum_{i_1}^{6}(-1)^i k\cdot a_i}$, $z^N = e^{\imath N\sum_{i_1}^{6}k\cdot a_i}$, and the new Hamiltonian is homotopic to the one obtained by post-composing with this map. We will also discuss the computation of the degree of such maps via the ray method in the very similar model of honeycomb lattices; see (30).

5.1.5. Criteria for choosing distant neighbors in a triangular lattice

Putting any integer N in Eq. will give a valid Hamiltonian with a Chern number $3N^2$. However, this Hamiltonian will not correspond to the tight-binding Hamiltonian at that new distance as the number and direction of neighbors change with distance in a triangular lattice as presented in Fig. 5(b). Commensurate lattices are given by $N = 3^{b_0}p_1^{b_1}p_2^{b_2}\dots p_c^{b_c}$, where N is the product of rational inert primes $p_i \equiv 2 \pmod 3$, §4.2.2. The first few integers are then $N \in \{1,2,3,4,5,6,9,10,\dots\}$. If we multiply the range of interactions t_1 and t_2 by these integers, we will get a new model that does not break the symmetry of the lattice, and that has $C = N^2$ times the original one. If we only multiply the range of t_1 terms, we get a Hamiltonian that has $C = N$ times the original one.

Example 5.1. Consider neighbors at distances 2 times that of the nearest neighbors. This corresponds to $t_1 \mapsto t_3$ and $t_2 \mapsto t_6$. This implements Eq. with $N = 2$ and will result in a model with Chern number $C = (2^2)\cdot 3 = 12$ since the original model with $N = 1$ had $C = 3$. Another construction is to leave t_2 the same and change the interaction $t_1 \mapsto t_3$, t_5 or t_9. This will implement Eq. with $N = 2, 3$ and 4 respectively, and will result in models with Chern numbers 6,9 and 12.

5.1.6. Honeycomb lattice

The honeycomb lattice received a lot of attention as it was the primary example of a tight-binding topological insulator without an external magnetic field [11]. Many physics papers studied instances of increasing the range of hopping to obtain higher Chern numbers [15,19,27]. As an example, for the third nearest neighbor, we have the following Hamiltonian:

$$h_1^{3rd\,NN}(k) = \sum_{i=1}^{3}\cos\left(k\cdot a_i\right) + t_3\sum_{i=1}^{3}\cos\left(k\cdot c_i\right), h_2^{3rd\,NN}(k) = \sum_{i=1}^{3}\sin\left(k\cdot a_i\right) + t_3\sum_{i=1}^{3}\sin\left(k\cdot c_i\right)$$
$$h_3^{3rd\,NN}(k) = m - 2t_2\sin(\phi)\sum_{i=1}^{3}\sin\left(k\cdot b_i\right) \tag{28}$$

Here, a_i and b_i denote the first and second-nearest neighbors vectors, respectively, while the new vectors c_i are the third-nearest neighbors. The phase diagram is shown in Fig. 8. The Hamiltonian remains 2×2, and the h_3 component remained the same because the third nearest neighbors are of the opposite species to the central atom. The third-nearest neighbor model hosts a phase with a Chern number $C = 2$ [15]. From the correspondence between the Chern number and the mapping degree, the image of the mapping $H(k) : T^2 \to \mathbb{R}^3$ has to have degree 2 for the corresponding points in the phase diagram Fig. 8 (obtained by direct integration). For example, the image of the map for $m = 0$, $\phi = \frac{\pi}{2}$ and $t_3 = 0.35$ is shown in Fig. 9. The map's restriction to the plane $h_3(k) = 0$ is isotopic to the rose curve shown in Fig. 1(d) with $d = 1$, $d' = -2$ and $t = \frac{1}{4}$. Here, the isotopy preserves the intersection points and fixes these at 0.

We remark that calculating the Chern number using the connection involves numerically evaluating a complicated integral. Analytically, we can compute the map degree from the ray method. However, this involves solving increasingly higher-degree polynomials, which becomes impractical after the fourth nearest-neighbor [15]. Moreover, the construction of these high Chern number models depends on tuning the interaction parameters to obtain a slice with high Chern numbers. This becomes increasingly harder as the dimension of the parameter space increases with each new interaction. However, applying the method of commensurate sublattices, we obtain Hamiltonians with a higher Chern number for Graphene in a simpler way. The resulting Hamiltonian when considering neighbors that are N times further than first-nearest neighbors is then:

$$h_1^{[C=N^2]}(k) = \sum_{i=1}^{3}\cos\left(k\cdot Na_i\right) = \sum_{i=1}^{3}\cos\left(Nk\cdot a_i\right), h_2^{[C=N^2]}(k) = \sum_{i=1}^{3}\sin\left(k\cdot Na_i\right) = \sum_{i=1}^{3}\sin\left(Nk\cdot a_i\right)$$
$$h_3^{[C=N^2]}(k) = m - 2t_2\sin(\phi)\sum_{i=1}^{3}\sin\left(k\cdot Nb_i\right) = m - 2t_2\sin(\phi)\sum_{i=1}^{3}\sin\left(Nk\cdot b_i\right) \tag{29}$$

The distant neighbors effectively implement the mapping $f_{d_1,d_2} : T^2 \to T^2, (\theta_1,\theta_2) \mapsto (d_1\theta_1, d_2\theta_2)$ whose degree is d_1d_2. Here, $d_1 = d_2 = N$ and the resulting Hamiltonian has a Chern number $C = N^2$. Concretely, in the Haldane model, we can take the interactions at a distance $N = 4$ multiples of the original. Assuming that the side of the hexagon has length 1, then we consider the blue atoms at distance 4 and the red atoms at distance $4\sqrt{3}$. It can be checked explicitly that there are only three blue atoms and six red atoms at these distances. Further, their vectors are just an integer multiple of the original Haldane model with distances 1, $\sqrt{3}$; see Fig. 10(a).

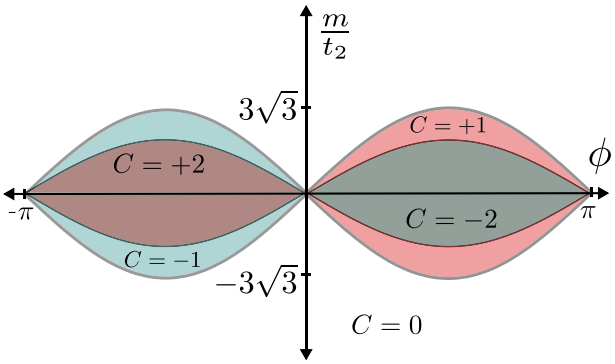

Fig. 8. Phase diagram of the Haldane model with third-nearest neighbors $t_1 = 1, t_2 = 0.5,\ t_3 = 0.35$ in Eq. (28). The Chern number takes higher values -2,2 for a specific region of parameters ϕ and m.

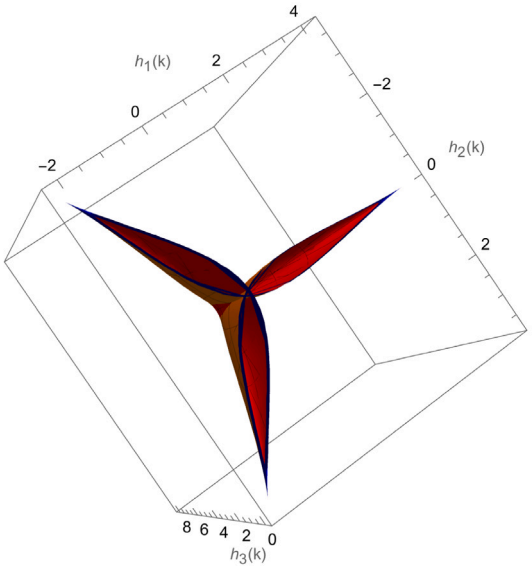

Fig. 9. The image of the map $H(k) : T^2 \to \mathbb{R}^3$ for $m = 0$, $\phi = \frac{\pi}{2}$, $t_2 = 0.5$ and $t_3 = 0.35$. The map has a degree 2 as any ray starting from the origin will intersect the surface twice. The highlighted plane $h_3(k) = 0$ is isotopic to the rose curve in Fig. 1(d), also fixing the origin as the sole crossing point in the isotopy.

5.1.7. Criteria for choosing distant neighbors in honeycomb lattice

The honeycomb lattice can be viewed as a subset of a triangular lattice with two species (the red and blue circles) while missing the third species (the hollow purple circles) as depicted in Fig. 10(a). The criteria for choosing N (the integer multiple of the distant neighbors) again follows the recipe for a triangular lattice §4.2.2 but with the additional constraint that we want to avoid fictitious lattice points at that distance. For example, we cannot extend the $A - B$ t_1 interaction by either $N = 2, 5$ or more generally $N > 0$ and $N \equiv 2 \pmod 3$ as at these distances there are no atoms in the same direction as the first nearest neighbors. However, for the negative values $N = -2, -5$, we have atoms at these distances, and we can choose N in these numbers. Further, since the Chern number is odd in N and ϕ, flipping both of them produces models with a positive Chern number.

5.1.8. A second basic model for honeycomb lattices

In the previous subsection, we implemented the construction of higher-Chern-number models by looking for distant neighbors that preserve the structure of the original Hamiltonian. In honeycomb lattices, we can also construct models that only preserve the $A - B$ interaction terms. Such models should be of practical value as the complex interactions $A - A$ and $B - B$ are harder to implement experimentally. The new Hamiltonian will be:

$$h_1^{[C=N]}(k) = \sum_{i=1}^{3} \cos\left(Nk \cdot a_i\right), \quad h_2^{[C=N]}(k) = \sum_{i=1}^{3} \sin\left(Nk \cdot a_i\right)$$

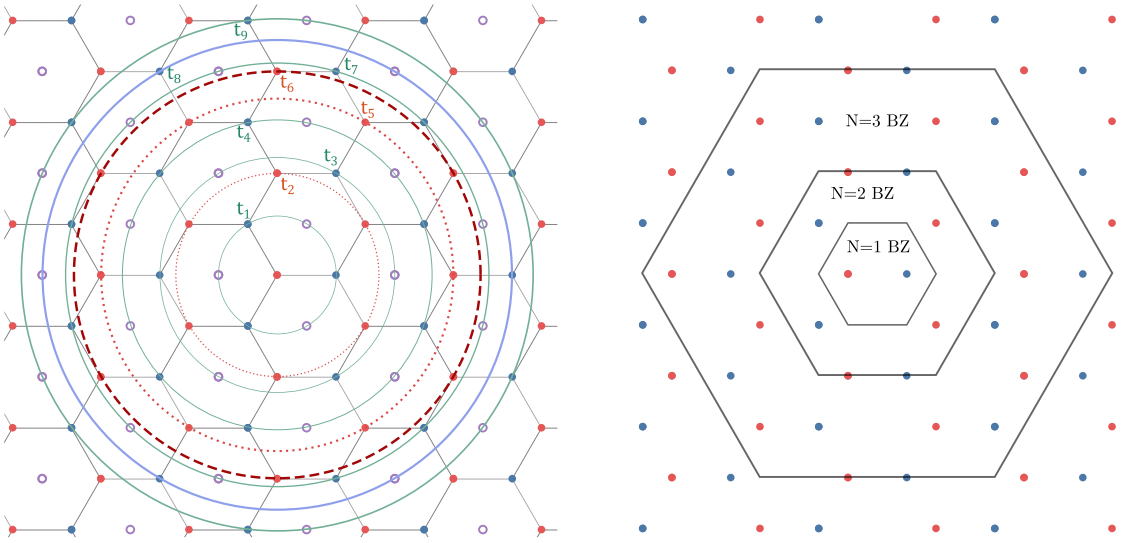

(A) The number and orientation of nearest neighbors in a Honeycomb lattice varying with distance. The choices of N. The K-like and K'-like points (blue and purple circles are drawn to exhibit the honeycomb as a subset of a triangular lattice. The original Hal- red, respectively) form a honeycomb lattice in mo- dane model uses t_1, t_2 interactions. Commensurate mentum space. It is evident geometrically that there are N^2 pre-Dirac points compared to the $N = 1$ case interactions with higher degree arise for neighbors at (the points at the boundary are identified because of distances 2 or 4 times that of nearest neighbors (t_1 periodic boundary conditions).
terms); these correspond to t_3 or t_8 and Chern num-
ber 2, 4, respectively. These are instances of Eq. (30).

(B) The structure of the pre-Dirac points for different

Fig. 10. Honeycomb lattice.

$$h_3^{[C=N]}(k) = m - 2t_2 \sin(\phi) \sum_{i=1}^{3} \sin\left(k \cdot b_i\right) \tag{30}$$

We can compute the Chern number of this model using the ray method; see §2.1.5. We draw a ray from the origin in the z direction and count how many times it intersects the surface generated by the Hamiltonian $H(k)$ in $\mathbb{R}^3$ as the momentum traverses the T^2 Brillouin zone. We can also extend the ray into a straight line and divide by 2.

$$C_1 = \sum_{p \in h^{-1}(q)} \operatorname{sgn}(\phi_p) = \frac{1}{2} \sum_{\substack{k \in \text{ BZ} \\ h_1(k)=h_2(k)=0}} \operatorname{sgn}\Big[(\partial_{k_x} h(k) \times \partial_{k_y} h(k)) \cdot \hat{z}\Big] \operatorname{sgn}\big[h_3(k)\big]. \tag{31}$$

The points satisfying $h_1(k) = h_2(k) = 0$ are the pre-Dirac points §2.1.5. In the original model with $N = 1$, these pre-Dirac points form on a honeycomb lattice with translation vectors: $\vec{g}_1 = \left(\frac{2\pi}{\sqrt{3}}, \frac{2\pi}{3}\right)$, $\vec{g}_2 = \left(-\frac{2\pi}{\sqrt{3}}, \frac{2\pi}{3}\right)$. Restricting to the first Brillouin Zone, we find only two terms $K = (\frac{4\pi}{3\sqrt{3}}, 0)$ and $K' = (\frac{-4\pi}{3\sqrt{3}}, 0)$ shown as blue and red circles respectively in Fig. 10(b). Since the new Hamiltonian terms ($h_1(k)$ and $h_2(k)$) are formed by composing the old terms by the map $k \mapsto Nk$, the new pre-Dirac points consist of the old pre-Dirac points but in an extended BZ. Since the new BZ is N^2 larger, it has N^2 more pre-Dirac points. For a model with a general N, the new N^2 pre-Dirac points are explicitly:

$$\{k \mid h_1^{[C=N]}(k) = h_2^{[C=N]}(k) = 0\} = \left\{ \tfrac{K + m\vec{g}_1 + n\vec{g}_2}{N}, \ \tfrac{K' + m\vec{g}_1 + n\vec{g}_2}{N} \ \middle| \ 0 \le m, n \le N-1 \right\}. \tag{32}$$

These vectors differ by an unimportant shift from the ones depicted in Fig. 10(b). Note that the sign of the first term $sgn\left[(\partial_{k_x} h(k) \times \partial_{k_y} h(k)) \cdot \hat{z}\right]$ is inherited from the original BZ (or inverted if N is negative). The first Chern number for the new Hamiltonian is then:

$$C_1 = \frac{1}{2} \sum_{\substack{0 \le m \le N-1 \\ 0 \le n \le N-1}} \left[\operatorname{sgn}\Big(h_3\Big(\frac{K + m\vec{g}_1 + n\vec{g}_2}{N}\Big)\Big) - \operatorname{sgn}\Big(h_3\Big(\frac{K' + m\vec{g}_1 + n\vec{g}_2}{N}\Big)\Big) \right]. \tag{33}$$

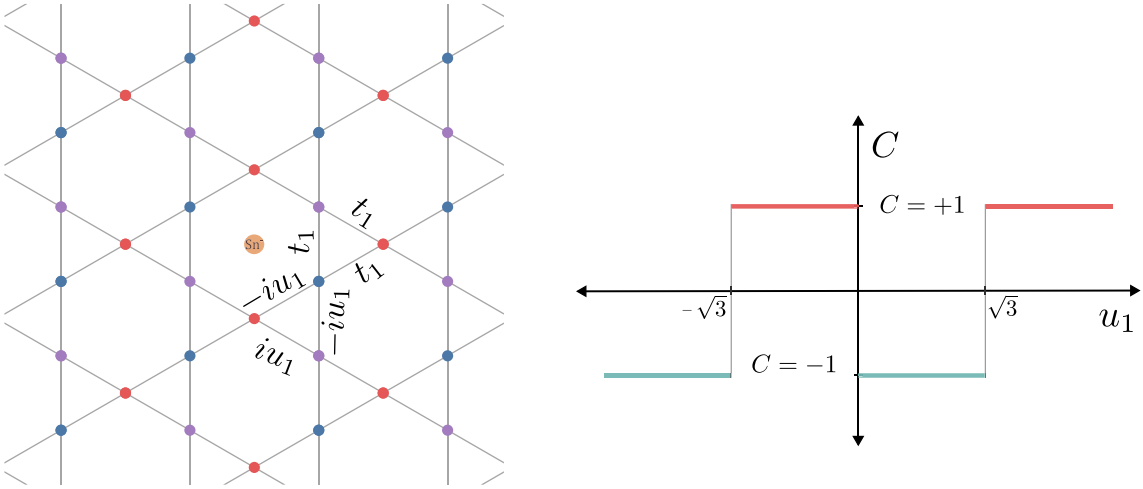

(A) A model for a Chern insulator on a Kagome lattice. First-nearest interactions are both real and imaginary. The complex interactions arise from the spin-orbit coupling of the electric field of the Sn ion at the center. Blue, red, and purple circles correspond to A, B, and C atoms in the Hamiltonian Eq. (36).

(B) One-dimensional phase diagram of the model for the ground state of the Kagome lattice Eq. (36) with $t_1 = 1$. The model is gapless for $u_1 \in \{\pm\sqrt{3}, 0\}$, otherwise it is gapped.

Fig. 11. Kagome lattice Hamiltonian terms (left) and phase diagram (right).

We can change the BZ for the second sum by $(\vec{g}_1, \vec{g}_2) \mapsto (-\vec{g}_1, -\vec{g}_2)$. This is just a reordering of the old vectors. The sum then becomes

$$C_1 = \frac{1}{2} \sum_{\substack{0\le m\le N-1\\ 0\le n\le N-1}} \left[\operatorname{sgn}\Big(h_3\Big(\frac{K + m\,\vec{g}_1 + n\,\vec{g}_2}{N}\Big)\Big) - \operatorname{sgn}\Big(h_3\Big(\frac{K' - m\,\vec{g}_1 - n\,\vec{g}_2}{N}\Big)\Big)\right]. \tag{34}$$

We specialize to the case $m = 0$ (this is m in (30), not to be confused with the dummy integer here), $\phi = \frac{\pi}{2}$, and $t_2 = \frac{1}{2}$. Thus $h_3(k) = \sum_{i=1}^{3} \sin\left(k \cdot b_i\right)$ is an odd function of k. This, together with the fact that $K' = -K$, simplifies the expression to: $C_1 = \sum_{0\le m,n\le N-1} sgn[h_3(\frac{K+m\vec{g}_1+n\vec{g}_2}{N})]$. Using the explicit form of $h_3(k)$, we arrive at:

$$C_1 = \sum_{\substack{0\le m\le N-1\\ 0\le n\le N-1}} \operatorname{sgn}\left[\left(\cos\left(\frac{(m+n)\pi}{N}\right) - \cos\left(\frac{(2-3m+3n)\pi}{3N}\right)\right) \qquad \sin\left(\frac{(2-3m+3n)\pi}{3N}\right)\right] = N. \tag{35}$$

We note that changing $m \leftrightarrow n$ changes the sign of the expression for $m \neq n$ and $m, n > 0$. Furthermore, the expression is negative if $m = n \neq 0$ and positive when $mn = 0$. These observations show that $C_1 = N$ for any N. It is worth noting that the Haldane model for 3rd-nearest neighbor (28) is an example of this family of Hamiltonians since the 3rd-nearest neighbors have the same structure as the 1st-nearest neighbors but with $N = -2$. see Fig. 8.

5.1.9. Kagome lattice

The same methods can be applied to Kagome lattices. As a concrete example, consider the Hamiltonian describing an interaction in a 3-species Kagome lattice, see Fig. 11(a):

$$\begin{aligned} H = &- t_1 \sum_{\langle i,j\rangle} (c^\dagger_{i,A} c_{j,B} + c^\dagger_{i,A} c_{j,C} + c^\dagger_{i,B} c_{j,C}) + iu_1 \sum_{\langle i,j\rangle} (c^\dagger_{i,A} c_{j,B} - c^\dagger_{i,A} c_{j,C} + c^\dagger_{i,B} c_{j,C}) \\ &+ h.c. \end{aligned} \tag{36}$$

As before, $\langle i, j\rangle$ denotes summation over first-nearest neighbors. This Hamiltonian is adapted from the Hamiltonian:

$$H = -t_1 \sum_{\langle ij\rangle\sigma} c^\dagger_{i\sigma} c_{j\sigma} + iu_1 \sum_{\langle ij\rangle\alpha\beta} \left(\mathbf{E}_{ij} \times \mathbf{R}_{ij}\right) \cdot \boldsymbol{\sigma}_{\alpha\beta} c^\dagger_{i\alpha} c_{j\beta} \tag{37}$$

Here, α and β represent spin indices, $\mathbf{R}_{ij}$ are the displacement vectors between sites i and j, and $\mathbf{E}_{ij}$ is the electric field from neighbors along $\mathbf{R}_{ij}$. This is a model for Fe_3Sn_2, and the second term is the spin–orbit coupling from the Sn ion at the center of the hexagon [53]. We obtain Eq. (36) after restricting to the spin-up electrons. The model is presented in Fig. 11(a). For another model that admits the same construction, see [54].

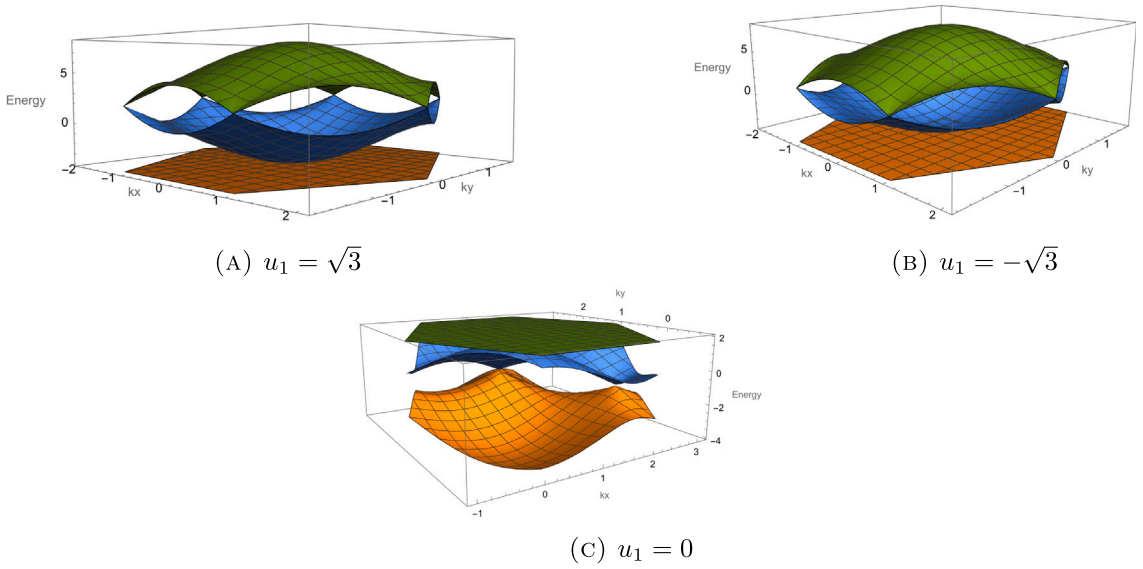

Fig. 12. The bands and critical points for $t_1 = 1$. For the lowest and 2nd lowest band: (A) at $u_1 = -\sqrt{3}$, one charge 2 point plotted at the center of the unit cell, (B) at $u_1 = \sqrt{3}$, one charge 2 point plotted at the center of the unit cell, and (C) at $u_1 = 0$, two Dirac points.

In Fig. 11(a), we denoted A, B, and C atoms using blue, red, and purple circles, respectively. After the Fourier transform, the resulting Hamiltonian is:

$$H(k) = -2t_1 \begin{pmatrix} 0 & \cos(k\cdot a_1) & \cos(k\cdot a_2) \\ \cos(k\cdot a_1) & 0 & \cos(k\cdot a_3) \\ \cos(k\cdot a_2) & \cos(k\cdot a_3) & 0 \end{pmatrix} + 2iu_1 \begin{pmatrix} 0 & \cos(k\cdot a_1) & -\cos(k\cdot a_2) \\ -\cos(k\cdot a_1) & 0 & \cos(k\cdot a_3) \\ \cos(k\cdot a_2) & -\cos(k\cdot a_3) & 0 \end{pmatrix}$$

The vectors $\{a_i\}$ represent the first-nearest neighbors' displacements. The Hamiltonian is gapless when $u_1 = 0, \pm\sqrt{3}$ otherwise, it is gapped. The Chern number for the lowest band can be computed by using direct integration of the connection (we also validated using the ray method §2.1.5), and it is found to be -1 when $t_1 = u_1 = 1$. A 1-d slice for the parameters is shown in Fig. 11(b).

Since this is a three-band system, there could be a jump by 2 stemming from three bands crossing, a jump by two from a higher local charge in a two-band crossing, or, generically, by two Dirac points with local charge 1. The three-band crossing is not realized, but (fixing $t_1 = 1$) for the lowest two bands at $u_1 = \pm\sqrt{3}$, there is one singular point whose local charge is 2. At $u_1 = 0$. The situation is the generic case of two Dirac points. This can be seen from a local analysis; see Fig. 12. Note that the 2nd and 3rd bands have the flipped behavior, i.e. two points at $\pm\sqrt{3}$ and one local charge 2 point at 0.

We can also expand the Hamiltonian in terms of Gell–Mann matrices since they span traceless Hermitian 3×3 matrices. We used the following ordering for the Gell–Mann matrices:

$$\begin{aligned} \lambda_1 &= \begin{pmatrix} 0 & 1 & 0 \\ 1 & 0 & 0 \\ 0 & 0 & 0 \end{pmatrix}, \quad \lambda_2 = \begin{pmatrix} 0 & -i & 0 \\ i & 0 & 0 \\ 0 & 0 & 0 \end{pmatrix}, \quad \lambda_3 = \begin{pmatrix} 1 & 0 & 0 \\ 0 & -1 & 0 \\ 0 & 0 & 0 \end{pmatrix}, \\ \lambda_4 &= \begin{pmatrix} 0 & 0 & 1 \\ 0 & 0 & 0 \\ 1 & 0 & 0 \end{pmatrix}, \quad \lambda_5 = \begin{pmatrix} 0 & 0 & -i \\ 0 & 0 & 0 \\ i & 0 & 0 \end{pmatrix}, \quad \lambda_6 = \begin{pmatrix} 0 & 0 & 0 \\ 0 & 0 & 1 \\ 0 & 1 & 0 \end{pmatrix}, \\ \lambda_7 &= \begin{pmatrix} 0 & 0 & 0 \\ 0 & 0 & -i \\ 0 & i & 0 \end{pmatrix}, \quad \lambda_8 = \frac{1}{\sqrt{3}} \begin{pmatrix} 1 & 0 & 0 \\ 0 & 1 & 0 \\ 0 & 0 & -2 \end{pmatrix}. \end{aligned} \tag{38}$$

The Hamiltonian in momentum space can be written as $H(k) = h'(k)\cdot\lambda$, where λ is an 8-dimensional vector of Gell–Mann matrices.

$$\begin{aligned} h'(k) = (&-2t_1\cos k_x, -2u_1\cos k_x, 0, -2t_1\cos(\frac{k_x+\sqrt{3}k_y}{2}), \\ &2u_1\cos(\frac{k_x+\sqrt{3}k_y}{2}), -2t_1\cos(\frac{k_x-\sqrt{3}k_y}{2}), -2u_1\cos(\frac{k_x-\sqrt{3}k_y}{2}), 0)^T \end{aligned} \tag{39}$$

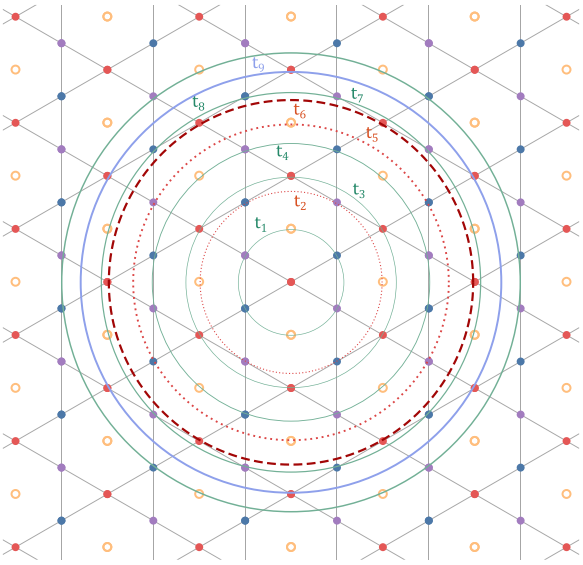

Fig. 13. The structure of the nearest-neighbor interactions in the Kagome lattice. The gold hollow circles represent fictitious points that complete the lattice into a triangular lattice. For certain ranges, the structure of the first-nearest neighbors appears again. For example, t_5 has the same structure as t_1. Thus, using $N = 3$ in Eq. (41) is a valid instance.

It should be noted that the coefficients can be arranged as:

$$\begin{aligned} H(k) = &\cos(k_x)[-2t_1\lambda_1 - 2u_1\lambda_2] + \cos(\frac{k_x + \sqrt{3}k_y}{2})[-2t_1\lambda_4 + 2u_1\lambda_5] \\ &+ \cos(\frac{k_x - \sqrt{3}k_y}{2})[-2t_1\lambda_6 - 2u_1\lambda_7] \end{aligned} \tag{40}$$

In this form, it is evident that the target space is a 3-dimensional subspace of $\mathbb{R}^8$ which depends on t_1 and u_1. Furthermore, since the eigenfunctions do not depend on the overall scale of the Hamiltonian, in the non-degenerate case, we can normalize $h(k)$ to $\hat{h}(k)$, establishing the target space as $S^2 \subset \mathbb{R}^3 \subset \mathbb{R}^8$. We can then use the results of §2.1.3 to calculate the Chern number directly by using a connection. This yields the Chern numbers $c_1 = \pm 1, 0$ with -1 for the lowest band.

By the general Theorem 2.2, this bundle is then isomorphic to the pull-back of a Spin 1 bundle. For this notice that there is a homotopy of the Hamiltonian which takes the coefficient $t_1 \to 0$ and keeps u_1 fixed. As long as u_1 was not critical, the homotopy does not cross the degeneracy locus, and hence the Chern number stays constant. Keeping only the u_1 terms, the Hamiltonian is a Spin–1 Hamiltonian. With the identification of $S_z = \lambda_2, S_y = \lambda_5, S_x = \lambda_7$, whose Chern classes are known. Note, this is simply i times the standard $\mathfrak{so}(3)$ representation $S_j = iL_j$. Then the computation of the Chern class reduces to the degree of the map defined by the coefficients in (40), which is 1.

Using the method of commensurate sublattices, the Hamiltonian is modified to:

$$\begin{aligned} H^{[C=N^2]}(\mathbf{k}) = &-2t_1 \begin{pmatrix} 0 & \cos(Nk\cdot a_1) & \cos(Nk\cdot a_2) \\ \cos(Nk\cdot a_1) & 0 & \cos(Nk\cdot a_3) \\ \cos(Nk\cdot a_2) & \cos(Nk\cdot a_3) & 0 \end{pmatrix} \\ &+ 2iu_1 \begin{pmatrix} 0 & \cos(Nk\cdot a_1) & -\cos(Nk\cdot a_2) \\ -\cos(Nk\cdot a_1) & 0 & \cos(Nk\cdot a_3) \\ \cos(Nk\cdot a_2) & -\cos(Nk\cdot a_3) & 0 \end{pmatrix}. \end{aligned} \tag{41}$$

This Hamiltonian will have a Chern number $C = N^2$.

5.1.10. Criteria for choosing distant neighbors in Kagome lattice

The Kagome lattice can be viewed as a subset of a triangular lattice with three species (blue, red, and purple circles) while missing the hollow gold circles as depicted in Fig. 13. To avoid breaking the lattice symmetry, N should be chosen such that the resulting neighbors at distance N have the same number and type as the original model. The criteria for choosing N (the integer multiple of the distant neighbors) again follow the recipe for a triangular lattice §4.2.2, but with the additional constraint that we want to have the same number of fictitious points at that distance as the original model. For example, we cannot extend the t_1 interaction by either $N = 2, 4$ or more generally $N > 0$ and $N \equiv 0 \pmod 2$ as at these distances the atoms in the same direction as the first nearest neighbors are of the same species as the central atom. The criteria is then to have $N \equiv 1 \pmod 2$ on top of the usual constraint: $N = 3^{b_0} p_1^{b_1} p_2^{b_2} \dots p_c^{b_c}$, where N is the product of rational inert primes $p_i \equiv 2 \pmod 3$ as discussed in §4.2.2.

6. Conclusion and outlook

We provided a fundamental study of the possibility of having phase diagrams with arbitrary Chern numbers and arbitrary crossings between them. In addition, we reviewed different methods of computing Chern numbers in 2D topological insulators. It was shown that for two-band systems, there exists a simple equivalence between the fiber-bundle picture and the mapping degree picture using the standard $spin\frac{1}{2}$ family. For higher band systems, this is also possible, but one has to know both the pull-back map and the bundle structure of the pulled-back Hamiltonian. The description in terms of pull-backs also results in the rather simple ray method for computation of Chern classes and phase diagrams of given systems, as opposed to the integration of the connection over the whole T^2 Brillouin zone. Physically, this means that we do not need to compute the ground state wave function in order to know its Chern number §2.1.5.

This relationship also provided insight into constructing new models with higher Chern numbers. There are two main obvious ways to construct higher degree Hamiltonians: composing the domain space with a mapping to itself (e.g., $T^2 \to T^2$ in the case of a 2D periodic Brillouin zone) or composing with a mapping from the target space to itself (e.g., $S^2 \to S^2$ in the case of a Bloch sphere). The latter allowed us to construct arbitrary tame phase diagrams by pulling back the standard $spin\frac{1}{2}$ family of Hamiltonians by families of maps with prescribed mapping degree. This has potential applications in designing materials and quantum information theory, as the design question is now given by gluing together standard systems in a prescribed way using a finite amount of data. One feature is a minimal number of Dirac points appearing for each wall-crossing, which is what is expected generically, but now realized explicitly.

The former formalism, that is, coverings of the torus by itself, can be thought of as moving to super-cells that, for instance, appear in stacking. This can be naturally realized for lattice models by distant-hopping interaction terms in real space. The requirement that the new interactions have the same structure to ensure simple covering maps led to constraints on the range of allowed hoppings. The lattices at these distances should be commensurate, that is, simply scalings of the original lattice. This classification problem was solved for those lattices that are also quadratic integer lattices. The study then translates to questions about the existence of a representation of primes in certain quadratic forms [49]. This is controlled by the behavior of rational primes after extension as explained in Appendix A.

Another direction was to provide new maps for honeycomb and triangular lattices that implement intrinsically new mappings with a higher degree. These later maps should be of experimental value as they only extend the real interaction terms.

While the analysis here is readily applicable for lattices that correspond to quadratic integer domains, such as triangular and square lattices, many other types of lattices can be treated as easily with minor modifications. This is because such lattices are often a subset of the former lattices. For example, honeycomb, Kagome, and dice lattices can be completed into a triangular lattice, while Lieb, checkerboard (Planar Pyrochlore), and rectangular lattices (with a rational ratio between sides) can be completed into a square lattice. In this paper, we showed how honeycomb and Kagome lattices, as examples, can be treated using this construction. It should also be noted that one can use the methods here for lattices that consist of two superimposed lattices as well (e.g., a triangular lattice on top of a square lattice ..., etc.). Another direction for generalization that is readily accounted for by this construction is the number of bands. Since the main method of using larger commensurate sublattices to achieve higher-degree maps relies solely on composition in domain space (the Brillouin Zone), the construction applies to n-band systems, as evidenced by the three-band Kagome case, which required no new modifications. These investigations present a unified way to view many constructions in the physics literature in which higher-Chern-number models were constructed by distant hopping [15,19,24,27,28,44]. It also presents new, simpler models with high Chern numbers that should be useful in experiments for Chern insulators or fractional topological insulators.

CRediT authorship contribution statement

Ralph M. Kaufmann: Writing – review & editing, Writing – original draft, Funding acquisition. **Mohamad Mousa:** Writing – review & editing, Writing – original draft. **Birgit Wehefritz–Kaufmann:** Writing – review & editing, Writing – original draft.

Declaration of competing interest

The authors declare that they have no known competing financial interests or personal relationships that could have appeared to influence the work reported in this paper.

Acknowledgments

The authors are grateful for the funding support from the College of Science at Purdue University. R.K would like to acknowledge funding from the Simons Foundation, United States. We would also like to thank Shawn Cui and Sabre Kais for motivating and very helpful initial discussions, as well as Garth Simpson for inquiring about the possibility of direct phase transitions, which are now realized via rose-curves. Finally, we would like to thank the anonymous referees for their comments which helped improve the manuscript.

Appendix A. Quadratic integers

A.1. Introduction

A natural setting to study 2D lattices is as integers appearing in the extension of the field of rationals $\mathbb{Q}$ by the square root of a negative square-free integer $-d \in \mathbb{Z}^-$, i.e. $\mathbb{Q}[\sqrt{-d}]$. The algebraic integers $\mathcal{O}_{\mathbb{Q}[\sqrt{-d}]}$ of the field $\mathbb{Q}[\sqrt{-d}]$ is the integral closure of $\mathbb{Z}$ in $Q[\sqrt{-d}]$. They form an integral domain and further $\mathcal{O}_{\mathbb{Q}[\sqrt{-d}]} = \mathbb{Z}[\omega] = \{a + \omega b : a, b \in \mathbb{Z}\}$, where $\omega = \frac{1+\sqrt{-d}}{2}$ if $-d \equiv 1 \pmod 4$ and $\omega = \sqrt{-d}$ otherwise. This ensures that the domain $\mathbb{Z}[\omega]$ is integrally closed. We will use $\mathbb{Z}[\omega]$ in this definition; this is not to be confused with the third root of unity, which we discuss later.

Choosing an embedding of the algebraic closure $\overline{\mathbb{Q}} \to \mathbb{C}$ and using the correspondence between $\mathbb{C} = \mathbb{R}^2$ as real vector spaces, the quadratic integers will form a lattice in $\mathbb{C}$ that can be used to study physical lattices. For $-d \neq 0$, the resulting lattice Γ will be a lattice in $\mathbb{R}^2$ of the form:

$$\Gamma = \begin{cases} \mathbb{Z}(1,0) + \mathbb{Z}\left(\frac{1}{2}, \frac{\sqrt{d}}{2}\right), & \text{if } -d \equiv 1 \pmod 4, \\ \mathbb{Z}(1,0) + \mathbb{Z}(0, \sqrt{d}), & \text{Otherwise.} \end{cases} \tag{42}$$

A main tool in the study is the norm function $N : \mathbb{Z}[\omega] \to \mathbb{N}$ which is defined as $N(a+b\omega) = (a+b\omega)\overline{(a+b\omega)}$. Where the over-bar denotes conjugation: $\overline{(a+b\sqrt{h})} := (a - b\sqrt{h})$ for any $h \in \mathbb{Z}$. After embedding into $\mathbb{C}$ the conjugation corresponds to complex conjugation. Consequently, the norm function is non-negative, multiplicative, and equals the square of the Euclidean distance from the origin. This completes the identification of the quadratic integers $\mathbb{Z}[\omega]$ with the 2D lattice Γ [48,49,55].

Quadratic integers inherit many of the properties of the ring of integers $\mathbb{Z}$, however, certain properties fail to lift. For example, the domain $\mathbb{Z}[\sqrt{-5}]$ is not a unique-factorization domain (UFD). This is evidenced by the factorization: $6 = 2 \cdot 3 = (1 + \sqrt{-5})(1 - \sqrt{-5})$. Additionally, in the same domain, we have $5 = (-1) \cdot \sqrt{-5} \cdot \sqrt{-5}$ which means that the rational prime $5 \in \mathbb{Z}$ is now reducible. However, $\mathbb{Z}[w]$ is a Dedekind domain and any ideal factors uniquely into prime ideals [48]. A rational prime p can have three behaviors after the extension. First, it can remain a prime and its principal ideal (p) remains a prime ideal. In this case, it is called an inert prime. Second, it can ramify as the square of a single prime ideal $(p) = \mathfrak{p}_1^2$ with $\mathfrak{p}_1$ a prime ideal in $\mathbb{Z}[\omega]$. Third, it can split into two distinct prime ideals $(p) = \mathfrak{p}_1\mathfrak{p}_2$. The behavior of rational primes after extension is well-studied, and we cite the following theorems without a proof, see e.g. [48,49,56].

Theorem A.1. *Let $K = \mathbb{Q}(\sqrt{d})$ be a quadratic field, an odd rational prime p ramifies, splits or remains inert in the quadratic extension to the field K = iff $\left(\frac{d}{p}\right) = 0, 1, -1$ respectively, where the Legendre symbol can be computed as follows:*

$$\left(\frac{d}{p}\right) = \begin{cases} 0, & \text{if } p \mid d, \quad \textit{in this case } p \textit{ ramifies,} \\ 1, & \text{if } d^{\frac{p-1}{2}} \equiv 1 \pmod p, \quad \textit{in this case } p \textit{ splits,} \\ -1, & \text{if } d^{\frac{p-1}{2}} \equiv -1 \pmod p, \quad \textit{in this case } p \textit{ is inert.} \end{cases}$$

For ease of presentation, we treat the $p = 2$ case separately. We have the following theorem [48].

Theorem A.2. *Let $K = \mathbb{Q}(\sqrt{d})$ be a quadratic field with field discriminant $D = d$, if $d \equiv 1 \pmod 4$, or $D = 4d$ if $d \not\equiv 1 \pmod 4$. Then the rational prime 2 behaves as follows in $\mathcal{O}_{\mathbb{Q}[\sqrt{-d}]}$: if $2 \mid D$, then 2 ramifies, if $2 \nmid D$ and $d \equiv 1 \pmod 8$, then 2 splits, and if $2 \nmid D$ and $d \equiv 3 \pmod 8$, then 2 remains inert.*

A.2. General quadratic integer domains

In this section, we prove useful lemmata for a general integer domain that is not necessarily a unique factorization domain (UFD). These lemmata aim to establish a connection between the behavior of rational primes when lifted to quadratic integer domains and the geometric structure of the lattices of their respective types. Importantly, we want to find the distances from the origin at which only a unique lattice point exists up to lattice symmetry. These special distances offer a skeleton of exact points where Chern numbers are multiples of the original models as discussed in §5.

In the following, Greek letters are used for quadratic integers while Latin letters are reserved for rational numbers. The letters p, and π are used for rational primes and quadratic primes in their respective ring. We start with three lemmata that illustrate the structure of the norm function in relation to inert primes.

Lemma A.1. *In a quadratic integer ring $\mathbb{Z}[\omega]$, the norm function cannot represent any inert prime $p \in \mathbb{Z}$. (i.e., there is no number with norm p).*

Proof. Assume $\exists \alpha \in \mathbb{Z}[\omega]$ such that $N(\alpha) = p$, then $N(\alpha) = \alpha \cdot \overline{\alpha} = p$. This is a contradiction since p is an inert prime and neither α nor its conjugate are units. □

Lemma A.2. *In a quadratic integer ring $\mathbb{Z}[\omega]$, the only numbers with norm p^2 for an inert prime $p \in \mathbb{Z}$ are associates of p (i.e. p has an isolated norm).*

Proof. Assume $\exists \alpha \in \mathbb{Z}[\omega]$ such that $N(\alpha) = p^2$ and $p \nmid \alpha$, so that $N(\alpha) = \alpha \cdot \overline{\alpha} = p^2$. Since p is an inert prime, $p \mid \alpha \cdot \overline{\alpha}$ so either $p \mid \alpha$ or $p \mid \overline{\alpha}$. The first case leads to a contradiction, and we are then left with $p \mid \overline{\alpha}$. Write $\overline{\alpha} = p \cdot \mu$ for some number $\mu \in \mathbb{Z}[\omega]$. Taking conjugates, we have $\alpha = p \cdot \overline{\mu}$. Then again $p \mid \alpha$: Take the norm of $\alpha = p \cdot \overline{\mu}$ and use the multiplicativity of the norm $N(\alpha) = N(p) \cdot N(\overline{\mu}) = p^2 \cdot N(\overline{\mu}) = p^2$ and hence μ is a unit. This completes the proof. □

Note that the norm of irreducible elements can be a composite number in a non-UFD. For example, in $\mathbb{Z}[\sqrt{-5}]$, $N(1+\sqrt{-5}) = (1+\sqrt{-5})(1-\sqrt{-5}) = 6$. We, however, do have the following lemma.

Lemma A.3. *In a quadratic integer ring $\mathbb{Z}[\omega]$, if an inert prime $p \in \mathbb{Z}$ divides the norm of an irreducible $\alpha \in \mathbb{Z}[\omega]$, then $N(\alpha) = p^2$ and α is an associate of p.*

Proof. Assume $\exists \alpha \in \mathbb{Z}[\omega]$ such that $p \mid N(\alpha)$ and $p \nmid \alpha$. Let us write the norm of α as $N(\alpha) = \alpha \cdot \overline{\alpha} = p \cdot \mu$. Since p is an inert prime, $p \mid \alpha \cdot \overline{\alpha}$, it follows that $p \mid \alpha$ from the multiplicativity of conjugation or, equivalently, from the proof of Lemma A.2. We can then write $\alpha = p \cdot \nu$. However, since α is an irreducible ν must be a unit, and $N(\alpha) = p^2$. □

Ramified primes obey a modified versions of Lemmata A.1, A.2, and A.3. We first note that in some cases the ramified prime p ramifies as the square of non-principal ideals. For example, in $\mathbb{Z}[\sqrt{-5}]$, $(2) = (2, 1+\sqrt{-5})^2$. In this case, there is no number whose norm is 2. This is easily seen from the norm function $N(a + b\sqrt{-5}) = a^2 + 5b^2$.

Lemma A.4. *In a quadratic integer ring $\mathbb{Z}[\omega]$, if the norm function represents a ramified prime $p \in \mathbb{Z}$, then $p = u \cdot \pi^2$ for some prime $\pi \in \mathbb{Z}[\omega]$ and unit u.*

Proof. Since the norm function represents p, $\exists \alpha$ such that $N(\alpha) = \alpha \cdot \overline{\alpha} = p$. Taking ideals $(\alpha)(\overline{\alpha}) = (p)$. Since p ramifies, the ideal generated by it has the form $(p) = \mathfrak{p}_1^2$ for some prime ideal $\mathfrak{p}_1$. We then have $(\alpha)(\overline{\alpha}) = \mathfrak{p}_1^2$. Because quadratic integers are Dedekind domains, ideals factor uniquely into prime ideals. We then have $(\alpha) = (\overline{\alpha}) = \mathfrak{p}_1$, which means α is a prime (in Dedekind domains, a principal ideal is prime iff its generator is a prime), and $\alpha = u \cdot \overline{\alpha}$. □

Similar to the inert prime case, where the square of an inert prime was an inert norm, if a ramified prime is represented by the norm function, then it has an isolated norm.

Lemma A.5. *In a quadratic integer ring $\mathbb{Z}[\omega]$, if the norm function represents a ramified prime $p \in \mathbb{Z}$, then p is an isolated norm (all numbers with norm p are associates of each other).*

Proof. If $N(\alpha) = N(\beta) = p$ then α, β are primes by Lemma A.4 and further $\overline{\alpha} = u \cdot \alpha$, $\overline{\beta} = w \cdot \beta$ for units $u, w \in \mathbb{Z}[\omega]$. We then have $u \cdot \alpha^2 = w \cdot \beta^2$, and since α and β are primes, they have to be associates. □

The last lemma for inert primes fails to work in general for ramified primes. In $\mathbb{Z}[\sqrt{-5}]$, consider $N(1+\sqrt{-5}) = 6$. Even though the ramified prime 2 divides the norm of the irreducible $(1+\sqrt{-5})$, the norm is not exactly 2. We then have the modified version of Lemma A.3.

Lemma A.6. *In a quadratic integer ring $\mathbb{Z}[\omega]$, if a ramified prime $p \in \mathbb{Z}$ divides the norm of an irreducible $\alpha \in \mathbb{Z}[\omega]$, and this ramified prime is represented by the norm function, then $N(\alpha) = p$, and α is a prime.*

Proof. Start with an irreducible α such that $N(\alpha) = \alpha \cdot \overline{\alpha} = p \cdot c$ for some non-unit integer c. Using Lemma A.4, $p = u \cdot \pi^2$ for some prime $\pi \in \mathbb{Z}[\omega]$ with $\overline{\pi} = u \cdot \pi$. We then have $\alpha \cdot \overline{\alpha} = u \cdot \pi^2 \cdot c$. Since π is a prime, it divides α and also $\overline{\alpha}$ (because $\overline{\pi} = u \cdot \pi$). Thus $\alpha = \pi \cdot w$ for some number w, however, the norm function fixes w as a unit. □

The ring $\mathbb{Z}[\omega]$ is a Dedekind domain. In particular, it is a Noetherian domain, which implies it is an atomic domain, and each number can be written in terms of a finite set of irreducibles. The factorization into irreducibles can still be non-unique [48]. Using the previous Lemmata A.1, A.2, A.3, A.4, A.5, and A.6, we can identify a family of numbers that have isolated norms in any $\mathbb{Z}[\omega]$.

Theorem A.3. *In a quadratic integer ring $\mathbb{Z}[\omega]$, the number $d = \prod_{i=1}^{r} p_i^{b_i} \prod_{j=1}^{s} {\pi_j}^{c_j}$ has an isolated norm, where $p_i \in \mathbb{Z}$ is an inert prime and $\pi_j \in \mathbb{Z}[\omega]$ is a prime whose norm is a ramified prime $q_j \in \mathbb{N}$ and $b_i, c_j, r, s \in \mathbb{N}$.*

Proof. Assume $\exists \alpha \in \mathbb{Z}[\omega]$ such that $N(\alpha) = N(d)$. Since $\mathbb{Z}[\omega]$ is an atomic domain, we can write α in terms of (possible non-unique) non-associate irreducibles μ_k and a unit u: $\alpha = u \cdot \prod_{k=1}^{t} {\mu_k}^{m_k}$ with $t, m_k \in \mathbb{N}$. From the multiplicativity of the norm we have: $N(\alpha) = \prod_{k=1}^{t} N(\mu_k)^{m_k} = N(d) = \prod_{i=1}^{r} p_i^{2b_i} \prod_{j=1}^{s} {q_j}^{c_j}$. Since the norm is a map to $\mathbb{N}$, there is a unique factorization for the norm of each irreducible μ_k in terms of rational primes. In this factorization, only inert or ramified primes should appear as otherwise, if a split prime g appears, this will imply $g \mid \prod_{i=1}^{r} p_i^{2b_i} \prod_{j=1}^{s} {q_j}^{c_j}$ which is rejected since all p_i and q_j are either inert or ramified. This means that the norm of every irreducible μ_k only consists of powers of inert or ramified primes. Using Lemmata A.3 and A.6, the

norm of any such irreducible is $N(\mu_k) = {p'_i}^2$ for some inert prime $p'_i \in \mathbb{Z}$ or $N(\mu_k) = q'_k \in \mathbb{Z}$ for a ramified prime q'_k. Since the irreducibles are non-associates by construction, every norm contributes a distinct prime: $N(\mu_k) \neq N(\mu_l)$ for $k \neq l$. Let us reorder the irreducibles in one factorization of α according to their norm type: $N(\alpha) = \prod_{k=1}^{x} {p'_k}^{2m_k} \prod_{k=x+1}^{t} {q'_k}^{m_k}$ for some integer $0 \leq x \leq t$. We then have $\prod_{k=1}^{x} {p'_k}^{2m_k} \prod_{k=x+1}^{t} {q'_k}^{m_k} = \prod_{i=1}^{r} p_i^{2b_i} \prod_{j=1}^{s} {q_j}^{c_j}$. Finally, since $\mathbb{N}$ is a UFD, we have $x = r$, $t = x + s$, $m_k = b_i$ for $k \leq x$, and $m_k = c_j$ for $k > x$, and $p'_k = p_i$, $q'_k = q_j$ up to reordering of indices. This fixes $\alpha = u \cdot \prod_{i=1}^{r} p_i^{b_i} \prod_{j=1}^{s} \pi_j^{c_j}$ which is an associate of d. □

The results of this section can be restated in terms of the structure of the nearest neighbors for lattices described by a quadratic integer ring Eq. (42), which works only if the norm function can be interpreted as a distance for field extensions $\mathbb{Q}[\sqrt{-d}]$.

Corollary A.1. *In a full 2D lattice Γ described by a quadratic integer ring $\mathbb{Z}[\omega]$, there are exactly $|U|$ nearest neighbors to any lattice point lying at a Euclidean distance $d = \prod_{i=1}^{r} p_i^{b_i} \prod_{j=1}^{s} q_j^{c_j/2}$ where each p_i is an inert prime $p_i \in \mathbb{Z}$ in $\mathbb{Z}[\omega]$, and $q_j \in \mathbb{N}$ is a ramified prime represented by the norm function, $b_i, c_j, r, s \in \mathbb{N}$, and $|U|$ is the cardinality of the set of units in $\mathbb{Z}[\omega]$.*

The set of units U for each ring $\mathbb{Z}[\omega]$ is given by [48]:

$$U = \begin{cases} \{1, i, -1, -i\} & \text{for } \mathbb{Z}[i], \\ \{\pm 1, \pm\omega, \pm\omega^2\} & \text{for } \mathbb{Z}[\omega] \text{ with } \omega = \frac{-1+\sqrt{-3}}{2}, \\ \{1, -1\} & \text{otherwise.} \end{cases} \tag{43}$$

A.3. Unique factorization domains

In this section, we specialize to the case when the underlying domain is also a unique factorization domain (UFD). In this case, stronger results apply. As any number admits a unique factorization into primes, the prime factors determine if the norm is isolated or not. The cases where a quadratic integer ring with an imaginary field is a UFD are given by the following Stark–Heegner theorem [57,58].

Theorem A.4 (*Stark–Heegner*). *The quadratic imaginary number field $\mathbb{Q}$ $\mathbb{Z}[\sqrt{-d}]$ has a ring of integers which is a unique-factorization domain iff*

$$d \in \{-1, -2, -3, -7, -11, -19, -43, -67, -163\}.$$

Lemmata A.1,A.2, and A.3 discussing inert rational primes carry over without generalization. However, we have the following two lemmata for ramified and split primes.

Lemma A.7. *In a quadratic integer ring $\mathbb{Z}[\omega]$ which is a UFD, any ramified prime $p \in \mathbb{Z}$ is represented by the norm function, and this norm is isolated.*

Proof. The ideal generated by the rational prime p splits as $(p) = \mathfrak{p}_1^2$ for a prime ideal $\mathfrak{p}_1 \subset \mathbb{Z}[\omega]$. Since every Dedekind domain that is a UFD is also a PID (Principal Ideal Domain), we have $p = \pi_1^2$ with a prime $\pi_1 \in \mathbb{Z}[\omega]$. The norm function $N(p) = p^2 = N(\pi_1)^2$ fixes $N(\pi_1) = p$. This proves the first part. For the second part, use Lemma A.5. □

On the other hand, all split primes have non-isolated norms.

Lemma A.8. *In a quadratic integer ring $\mathbb{Z}[\omega]$ which is a UFD, any split prime $p \in \mathbb{Z}$ is represented by the norm function, and this norm is not isolated.*

Proof. The ideal generated by the rational prime p splits as $(p) = \mathfrak{p}_1\mathfrak{p}_2$ for two distinct prime ideals $\mathfrak{p}_1, \mathfrak{p}_2 \subset \mathbb{Z}[\omega]$. Since every Dedekind domain that is a UFD is also a PID, we have $p = \pi_1\pi_2$ for distinct primes $\pi_1, \pi_2 \in \mathbb{Z}[\omega]$. The norm function $N(p) = p^2 = N(\pi_1)N(\pi_2)$ fixes $N(\pi_1) = N(\pi_2) = p$ as otherwise one of them has to be a unit. This means in particular, $p = \pi_1\pi_2 = \pi_1 \cdot \overline{\pi_1}$. Hence, $\pi_2 = \overline{\pi_1}$. Finally, $\pi_1 \neq u \cdot \overline{\pi_1}$ for some unit u because, if this is the case, then p ramifies. □

Combining these lemmata with Theorem A.3, we have the following theorem.

Theorem A.5. *In a quadratic integer ring $\mathbb{Z}[\omega]$ which is a UFD, a number has an isolated norm iff its norm is not divisible by any split prime $p \in \mathbb{Z}$.*

Proof. Call such a number α. It has a unique factorization, $\alpha = \prod_{i=1}^{r} \pi_i^{m_i}$ into distinct primes $\pi_i \in \mathbb{Z}[\omega]$, and its norm is $N(\alpha) = \prod_{i=1}^{r} [N(\pi_i)]^{m_i}$. However, since each norm $N(\pi_i)$ only consists of inert or ramified primes, by Lemmata A.3 and A.8, this norm only comes from a unique number up to associates. This fixes any number with the same norm up to units. For the reverse direction, assume $p \mid N(\alpha)$ where $p \in \mathbb{N}$ is a split prime in $\mathbb{Z}[\omega]$. Then there is at least one prime π_j in the factorization of α such that $N(\pi_j) = p$. Write $\alpha = \pi_j \cdot \gamma$ for some number $\gamma \in \mathbb{Z}[\omega]$. By Lemma A.7, the number $\alpha' = \overline{\pi_j} \cdot \gamma$ has the same norm as and is not an associate to α. □

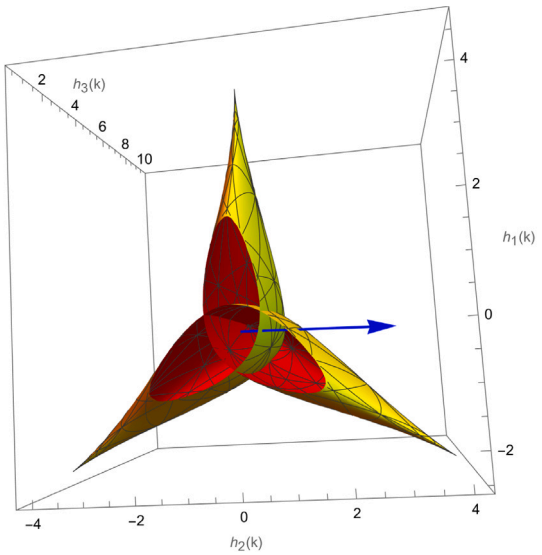

Fig. 14. The image of the map $H(k) : T^2 \to \mathbb{R}^3$ for $m = 2$, $\phi = 1.5$, $t_1 = t_2 = 1$, $t_3 = 0.5$, and $t_4 = t_5 = t_6 = 0$ in Eq. (45). The map has a degree 2 as evident by the intersections of the blue ray. Compare with Fig. 9.

Appendix B. Numerical validation of phase diagrams

In this section, we further strengthen the claims about the high-Chern-number phases obtained in the main text. In particular, we show that for representative examples, the new phases are robust under small perturbations. We further expand on the computational methodologies used to obtain the phase diagrams. We contrast the analytic method introduced in the text with the numerical methods, such as the ray method or direct Berry curvature integration.

B.1. Ray method computation

The ray method discussed in §2.1.5, computes the Chern number when it is equivalent to the covering degree from the torus T^2 to the sphere S^2; $f : T^2 \to S^2$. Intuitively, one can count this degree visually if the map is simple enough and when the image is not yet normalized (i.e., $Im(f) \in \mathbb{R}/\{0\}$. For a concrete example, let us look at the honeycomb model 5.1.6 with $t_1 = t_2 = 1$ and $t_3 = 0.5$, in Eq. (28). The image of the Hamiltonian map is shown in Fig. 14. A ray from the origin intersects the surface twice. Note also the different colors of the two faces of the surface, which indicate the direction they were traversed.

In fact, in almost all the situations discussed in this paper, this heuristic method provides a good estimate of the Chern number. For example, when the surface is clearly away from the origin, one can be sure that the Chern number is zero. To make this more automatable, let us use a generalized version of Eq. (31):

$$C_1 = \frac{1}{2} \sum_{\substack{k \in \text{ BZ} \\ h(k) \cap R}} \text{sgn}\Big[(\partial_{k_x} h(k) \times \partial_{k_y} h(k)) \cdot \hat{R}\Big]. \tag{44}$$

Here, $h(k)$ is the image of the Hamiltonian function, and R is the set of points on the straight line of the ray (one can actually just strictly use a ray and not divide by 2). Let us also consider the explicit Hamiltonian terms up to the sixth-nearest-neighbor term.

$$\begin{aligned} h_1^{\text{6th-NN}}(k) &= t_1 \sum_{i=1}^{3} \cos\left(k \cdot a_i\right) + t_3 \sum_{i=1}^{3} \cos\left(k \cdot c_i\right) + t_4 \sum_{i=1}^{6} \cos\left(k \cdot d_i\right), \\ h_2^{\text{6th-NN}}(k) &= t_1 \sum_{i=1}^{3} \sin\left(k \cdot a_i\right) + t_3 \sum_{i=1}^{3} \sin\left(k \cdot c_i\right) + t_4 \sum_{i=1}^{6} \sin\left(k \cdot d_i\right), \\ h_3^{\text{6th-NN}}(k) &= m - 2t_2 \sin(\phi) \sum_{i=1}^{3} \sin\left(k \cdot b_i\right) - 2t_5 \sin(\phi_5) \sum_{i=1}^{3} \sin\left(k \cdot e_i\right) - 2t_6 \sin(\phi_6) \sum_{i=1}^{3} \sin\left(k \cdot f_i\right). \end{aligned} \tag{45}$$

The vectors $\{a, b, \ldots, f\}$ are the $\{1^{\text{st}}, 2^{\text{nd}}, \ldots, 6^{\text{th}}\}$ nearest-neighbor vectors respectively, and the phases ϕ_5 and ϕ_6 are defined analogously to ϕ just as in Fig. 4(a). We can set $t_4 = t_5 = t_6 = 0$ in our current discussion, obtaining the model in Eq. (28) for 3rd nearest neighbors. The more general case will be used shortly in a following investigation of the gap analysis.

To get the Chern number using the ray method, Alg. 1 follows Eq. (44) closely. First, we input the Hamiltonian $h(k)$, any arbitrary ray intersecting the origin R *s.t.* $R \cap \{0\} = \{0\}$, and the bounds of the Brillouin Zone BZ. Second, since we have analytic equations

for the Hamiltonian terms, the whole Jacobian $J(k) = (\partial_{k_x} h(k) \times \partial_{k_y} h(k))$ can be precomputed as an analytic function of k_x, k_y. This is both more accurate and faster than using difference differentiation. Third, we find the momentum points in the Brillouin zone $q \in BZ$ satisfying $h(q) \cap R \neq \emptyset$. This amounts to solving $h(q) = \lambda R$ for a free variable $\lambda \in \mathbb{R}$, which are three equations in disguise for the three axes $h_i(k) = \lambda R_i$, where R_1 is the x-component of R, etc. This is the most crucial and computationally expensive step. Failure can happen here due to two main numerical reasons: (a) if the preimages are very close to the boundaries of the BZ, preimages may be undercounted or overcounted, (b) if the Jacobian vanishes (i.e., R is not a regular point [21,59]); see also §2.1.5. Fourth, for each preimage $q \in BZ$, we compute the Jacobian orientation relative to the surface $c = \mathrm{sgn}[J(\mathbf{q}) \cdot \mathbf{R}]$. In the fifth step, the candidate Chern number is calculated and checked. The two problems from step three can be detected when the number of intersections is odd, yielding a half-rational Chern number. Alternatively, we can simply it can also be checked by repeating the calculation with a randomly perturbed ray $R + \delta R$ or a slightly shifted BZ (by periodicity, it should give the same answer).

Algorithm 1 Computing Chern Number using Ray Method

Require: Hamiltonian map $h(k)$, a point defining the ray $R \in \mathbb{R}^3$, Brillouin Zone bounds BZ(k)
Ensure: Chern number C

procedure ChernByRay($h(k)$, R, BZ)
  Precompute the Jacobian $J(k) = (\partial_{k_x} h(k) \times \partial_{k_y} h(k))$
  loop
    Initialize $\mathrm{C}' \leftarrow 0$
    Find the set of all preimage momenta mapping to the ray: $Q = \{q \in \mathrm{BZ} \mid h(q) \in R\}$
    for each $q \in Q$ **do**
      Evaluate the local orientation $c \leftarrow \mathrm{sgn}[J(q) \cdot R]$
      $\mathrm{C}' \leftarrow \mathrm{C}' + c$
    end for
    if $\mathrm{C}' \equiv 0 \pmod 2$ **then** ▷ Intersections must be even
      break
    else
      Perturb $R + \delta R$ and shift $k + \delta k$ ▷ Constant shift of k effectively shifts the BZ
    end if
  end loop
  $\mathrm{C} \leftarrow \mathrm{C}'/2$ ▷ Since we used a straight line (we allowed $\lambda < 0$)
  return C
end procedure

B.2. Honeycomb $C \in \{-2, -1, 1, 4\}$ example

In this brief section, we investigate the robustness of the constructions introduced in Section 5. Namely, their gap and Chern number stability under perturbations.

Let us investigate the model introduced in Eq. (29) with $N = 2$. This model is a special case of the Hamiltonian in Eq. (45). It was shown analytically to have higher Chern numbers $+4, -4$ when $t_3 = t_6 = 1$ for varying m and ϕ_6, setting all other variables to 0. As this model will have the same phase diagram as the Haldane model Eq. (16) but scaled with $N^2 = 4$. This model can also realize a Chern number $C = \pm 2$ as shown in Fig. 8 using the parameters (with $N = 2$) in Eq. (30). We can test the robustness of this construction by simultaneously turning on the other parameters $t_1 = t_2 = \mathrm{v}$ and varying v. When $\mathrm{v} = 0$, we should recover the phase diagram in Fig. 4(b) scaled by 4, so we get $C = -4$ (choosing $m = 0$ and $\phi_6 = -1$). The gap, along with the Chern number, is shown in Fig. 15. Expectedly, when $|\mathrm{v}| \gg t_3, t_6$, the model recovers the phase diagram of the Haldane model Eq. (16) where only $C \in \{-1, +1\}$ is observed. The behavior here is typical for how our construction is to be used. The analytic point using the text's method $\mathrm{v} = 0$ acts as a beacon that guarantees a high-Chern point in the parameter space, the extent to which it persists has to be supplied by numerical computation.

For this phase diagram, we also double-checked with direct integration. The ray method was naturally found to be much faster than direct integration. In reality, one needs to check the Chern number only once inside any connected element of the phase diagram where no gap closes. This can be used to map the phase diagram more quickly (skipping the points where the gap is very small was also found to greatly improve performance). A small variation on Alg. 1 is then to perturb the Hamiltonian in order to move it to another equivalent point such that the gap remains open. We did not use this for the pseudocode we provided to keep it minimal. However, in practice, this can be utilized as well, and it drastically lowers the computational cost of constructing phase diagrams.

Data availability

No data was used for the research described in the article.

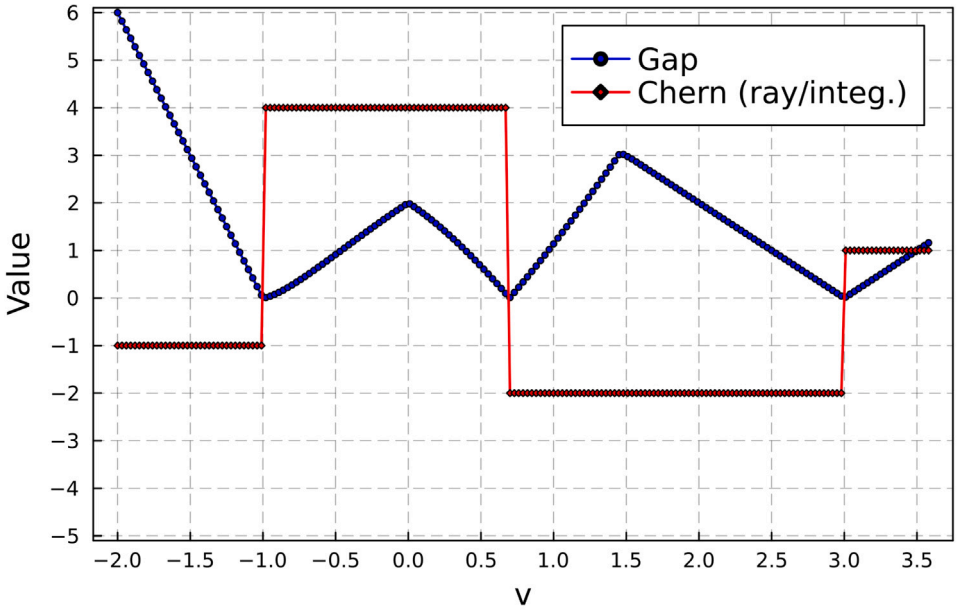

Fig. 15. The gap and Chern number for a slice of the Hamiltonian in Eq. (45) with $t_1 = t_2 = \mathrm{v}$, $t_3 = t_6 = 1$, $m = 0$, $\phi = 1$, and $\phi_6 = -1$. As expected, $C = -4$ when $\mathrm{v} = 0$. This persists for an extended interval until the gap closes, either at $\mathrm{v} = \pm 1$.

References

[1] A. Connes, Noncommutative Geometry, Academic Press, Inc., San Diego, CA, 1994, p. xiv+661.
[2] M. Aizenman, B. Nachtergaele, Geometric aspects of quantum spin states, Comm. Math. Phys. 164 (1) (1994) 17–63.
[3] J. Bellissard, A. van Elst, H. Schulz-Baldes, The noncommutative geometry of the quantum Hall effect, J. Math. Phys. 35 (10) (1994) 5373–5451, Topology and physics.
[4] T.A. Loring, *K*-theory and pseudospectra for topological insulators, Ann. Physics 356 (2015) 383–416.
[5] R. Moessner, J.E. Moore, Topological Phases of Matter, Cambridge University Press, 2021.
[6] A. Kapustin, Topological phases of matter and homotopy theory, in: Encyclopedia of Mathematical Physics, in: Condensed Matter and Statistical Physics & Classical and Quantum Gravity, vol. 1, Academic Press, Amsterdam, 2025, pp. 106–110, ©2025.
[7] M.V. Berry, Quantal phase factors accompanying adiabatic changes, Proc. R. Soc. Lond. 392 (1802) (1984) 45–57.
[8] D.J. Thouless, M. Kohmoto, M.P. Nightingale, M. den Nijs, Quantized Hall conductance in a two-dimensional periodic potential, Phys. Rev. Lett. 49 (6) (1982) 405–408.
[9] B. Simon, Holonomy, the quantum adiabatic theorem, and Berry's phase, Phys. Rev. Lett. 51 (24) (1983) 2167–2170.
[10] R.M. Kaufmann, S. Khlebnikov, B. Wehefritz-Kaufmann, Singular geometry of the momentum space: from wire networks to quivers and monopoles, J. Singul. 15 (2016) 53–79.
[11] F.D. Haldane, Model for a quantum Hall effect without Landau levels: Condensed-matter realization of the "parity anomaly", Phys. Rev. Lett. 61 (18) (1988) 2015–2018.
[12] H. Abdul-Rahman, M. Lemm, A. Lucia, B. Nachtergaele, A. Young, A class of two-dimensional AKLT models with a gap, in: Analytic Trends in Mathematical Physics, in: Contemp. Math., vol. 741, Amer. Math. Soc., [Providence], RI, 2020, pp. 1–21, ©2020.
[13] B. Nachtergaele, R. Sims, A. Young, Stability of the bulk gap for frustration-free topologically ordered quantum lattice systems, Lett. Math. Phys. 114 (1) (2024) Paper No. 24, 55.
[14] A. Cerjan, T.A. Loring, F. Vides, Quadratic pseudospectrum for identifying localized states, J. Math. Phys. 64 (2) (2023) Paper No. 023501, 21.
[15] D. Sticlet, F. Piéchon, Distant-neighbor hopping in graphene and Haldane models, Phys. Rev. B 87 (2013) 115402.
[16] B.A. Bernevig, T.L. Hughes, S.-C. Zhang, Quantum spin Hall effect and topological phase transition in Hg Te quantum wells, Science 314 (5806) (2006) 1757–1761.
[17] J.K. Asbóth, L. Oroszlány, A. Pályi, A short course on topological insulators: Band structure and edge states in one and two dimensions, in: Lecture Notes in Physics, vol. 919, Springer International Publishing, Cham, 2016.
[18] S. Yang, Z.-C. Gu, K. Sun, S. Das Sarma, Topological flat band models with arbitrary chern numbers, Phys. Rev. B 86 (2012) 241112.
[19] C. Bena, L. Simon, Dirac point metamorphosis from third-neighbor couplings in graphene and related materials, Phys. Rev. B 83 (2011) 115404.
[20] T.-W. Chen, Z.-R. Xiao, D.-W. Chiou, G.-Y. Guo, High chern number quantum anomalous Hall phases in single-layer graphene with Haldane orbital coupling, Phys. Rev. B 84 (2011) 165453.
[21] D. Sticlet, F. Piéchon, J.-N. Fuchs, P. Kalugin, P. Simon, Geometrical engineering of a two-band Chern insulator in two dimensions with arbitrary topological index, Phys. Rev. B 85 (2012) 165456.
[22] M. Fruchart, D. Carpentier, An introduction to topological insulators, Comptes Rendus. Phys. 14 (9–10) (2013) 779–815.
[23] S.-Y. Lee, J.-H. Park, G. Go, J.H. Han, Arbitrary chern number generation in the three-band model from momentum space, J. Phys. Soc. Japan 84 (6) (2015) 064005.
[24] Y.-X. Wang, J. Cao, Y.-M. Wu, Distant-neighbor hopping induced the Dirac points and the high Chern number topological phase on π -flux square lattice, Phys. Lett. A 379 (42) (2015) 2783–2788.
[25] A. Alase, D.L. Feder, Generating and detecting topological phases with higher Chern number, Phys. Rev. A 103 (2021) 053305.

[26] P.J. Ledwith, A. Vishwanath, E. Khalaf, Family of ideal Chern flatbands with arbitrary chern number in chiral twisted graphene multilayers, Phys. Rev. Lett. 128 (2022) 176404.
[27] S. Mondal, S. Basu, Topological phases of a semi-Dirac Chern insulator in the presence of extended range hopping, Phys. Rev. B 105 (2022) 235441.
[28] S. Woo, S. Woo, J.-W. Ryu, H.C. Park, Engineering high Chern number insulators, J. Korean Phys. Soc. 85 (8) (2024) 661–669.
[29] S.S. Dabiri, H. Cheraghchi, Construction of diverse two-dimensional models with arbitrary Chern number from one-dimensional models, Phys. Rev. B 112 (2025) 125418.
[30] F.D.M. Haldane, Continuum dynamics of the 1-D heisenberg antiferromagnet: Identification with the O(3) nonlinear sigma model, Phys. Lett. A 93 (9) (1983) 464–468.
[31] G. Grandi, Flores geometrici ex Rhodonearum, et Cloeliarum Curvarum Descriptione Resultantes, Typis Regiae Celsitudinis, Florence, Italy, 1728, p. 210.
[32] F. Hirzebruch, Topological methods in algebraic geometry, in: Die Grundlehren der mathematischen Wissenschaften, vol. Band 131, Springer-Verlag New York, Inc., New York, 1966, p. x+232, German ed.
[33] S. Kobayashi, K. Nomizu, Foundations of differential geometry. Vol. II, in: Interscience Tracts in Pure and Applied Mathematics, No. 15, Interscience Publishers John Wiley & Sons, Inc., New York-London-Sydney, 1969, p. xv+470.
[34] R. Bott, L.W. Tu, Differential forms in algebraic topology, in: Graduate Texts in Mathematics, vol. 82, Springer-Verlag, New York-Berlin, 1982, p. xiv+331.
[35] J.W. Milnor, Topology from the Differentiable Viewpoint, University Press of Virginia, Charlottesville, VA, 1965, p. ix+65, Based on notes by David W. Weaver.
[36] S. Smale, The classification of immersions of spheres in Euclidean spaces, Ann. of Math. (2) 69 (1959) 327–344.
[37] M.W. Hirsch, Immersions of manifolds, Trans. Amer. Math. Soc. 93 (1959) 242–276.
[38] R.M. Kaufmann, S. Khlebnikov, B. Wehefritz-Kaufmann, Local models and global constraints for degeneracies and band crossings, J. Geom. Phys. 158 (2020) 103892, 16.
[39] R.M. Kaufmann, D. Li, B. Wehefritz-Kaufmann, Topological insulators and K-theory, J. Math. Phys. 65 (4) (2024) Paper No. 043502, 34.
[40] R.M. Kaufmann, S. Khlebnikov, B. Wehefritz-Kaufmann, Singularities, swallowtails and Dirac points. An analysis for families of Hamiltonians and applications to wire networks, especially the gyroid, Ann. Physics 327 (11) (2012) 2865–2884.
[41] R.M. Kaufmann, D. Li, B. Wehefritz-Kaufmann, Notes on topological insulators, Rev. Math. Phys. 28 (10) (2016) 1630003, 57.
[42] G.M. Ziegler, Lectures on polytopes, in: Graduate Texts in Mathematics, vol. 152, Springer-Verlag, New York, 1995, p. x+370.
[43] X.-L. Qi, Y.-S. Wu, S.-C. Zhang, Topological quantization of the spin Hall effect in two-dimensional paramagnetic semiconductors, Phys. Rev. B 74 (2006) 085308, URL https://link.aps.org/doi/10.1103/PhysRevB.74.085308.
[44] Z. Wang, Y. Biao, X.-T. Zeng, X. Chen, X.-L. Sheng, S.A. Yang, R. Yu, Realization in circuits of a chern state with an arbitrary Chern number, Phys. Rev. B 107 (2023) L201101.
[45] R.M. Kaufmann, S. Khlebnikov, B. Wehefritz-Kaufmann, Re-gauging groupoid, symmetries and degeneracies for graph Hamiltonians and applications to the gyroid wire network, Ann. Henri PoincarÉ 17 (6) (2016) 1383–1414.
[46] R.M. Kaufmann, S. Khlebnikov, B. Wehefritz-Kaufmann, The geometry of the double gyroid wire network: quantum and classical, J. Noncommut. Geom. 6 (4) (2012) 623–664.
[47] F.D.M. Haldane, Nonlinear field theory of large-spin Heisenberg antiferromagnets: Semiclassically quantized solitons of the one-dimensional easy-Axis Néel state, Phys. Rev. Lett. 50 (1983) 1153–1156.
[48] K. Ireland, M. Rosen, A classical introduction to modern number theory, second ed. in: Graduate Texts in Mathematics, vol. 84, Springer-Verlag, New York, 1990.
[49] D.A. Cox, Primes of the Form $x^2 + Ny^2$: Fermat, Class Field Theory, and Complex Multiplication, Wiley, 1989.
[50] L. Euler, Demonstratio theorematis FERMATIANI omnem numerum primum formae $4n+1$ esse summam duorum quadratorum, Novi Comment. Acad. Sci. Petropolitanae 5 (1760) 3–13, Original version published in 1754/5.
[51] D. Zagier, A one-sentence proof that every prime $p \equiv 1 \pmod 4$ is a sum of two squares, Amer. Math. Monthly 97 (2) (1990) 144, JSTOR: 2323918, MR: 1041893.
[52] Y.-L. Wu, B.A. Bernevig, N. Regnault, Zoology of fractional Chern insulators, Phys. Rev. B 85 (2012) 075116.
[53] E. Tang, J.-W. Mei, X.-G. Wen, High-temperature fractional quantum Hall states, Phys. Rev. Lett. 106 (2011) 236802.
[54] K. Ohgushi, S. Murakami, N. Nagaosa, Spin anisotropy and quantum Hall effect in the kagomé lattice: Chiral spin state based on a ferromagnet, Phys. Rev. B 62 (2000) R6065–R6068.
[55] J.H. Conway, N.J.A. Sloane, Sphere Packings, Lattices and Groups, third ed. Springer-Verlag, 1999.
[56] J. Neukirch, Algebraic number theory, in: Grundlehren der mathematischen Wissenschaften, vol. 322, Springer-Verlag, Berlin, 1999.
[57] H.M. Stark, On the gap in the theorem of Heegner, J. Number Theory 1 (1) (1969) 16–27.
[58] H.M. Stark, A historical note on complex quadratic fields with class-number one, Proc. Amer. Math. Soc. 21 (1969) 254–255.
[59] K. Asano, C. Hotta, Designing Dirac points in two-dimensional lattices, Phys. Rev. B 83 (2011) 245125.